NEUTRON TOTAL CROSS SECTIONS
BY TIME-OF-FLIGHT

by

Raymond Morris Wilenzick

Date: August 20, 1958

Approved: H. W. Lewis
Henry W. Newson
J. M. Gallie, Jr.

A thesis

submitted in partial fulfillment
of the requirements for the
degree of Master of Arts
in the Graduate School
of Arts and Sciences
of
Duke University

1958

ACKNOWLEDGMENTS

I wish to express my gratitude to Dr. H. W. Lewis who suggested this project and who gave invaluable counsel throughout the experiment. Special thanks are due my colleagues in the time-of-flight group, Messers P. R. Bevington, G. E. Mitchell, and W. W. Rolland for their untiring assistance and for the use of certain apparatus of their design. I also wish to thank Dr. H. W. Newson for helpful discussions and Dr. K. K. Seth for his new method of area analysis. And, of course, I wish to express my appreciation to the entire Van de Graaff group who assisted in taking the data.

This work was supported by the Atomic Energy Commission.

R. M. W.

CONTENTS

LIST OF FIGURES

LIST OF TABLES

NEUTRON TOTAL CROSS SECTIONS
BY TIME-OF-FLIGHT

CHAPTER I

INTRODUCTION

The interaction of neutrons with nuclei may be quantitatively described in terms of the concept of cross section. The definition of the term cross section is given by Blatt and Weisskopf [1] as:

$$\sigma = \frac{\text{Number of events of a given type/ unit time/ nucleus}}{\text{Number of incident particles/ unit area/ unit time}}$$

The cross section is expressed in terms of a unit of 10^{-24} cm^2 called a barn.

The cross sections discussed in this paper are total cross sections, consisting primarily of elastic scattering but which also include any other processes which remove neutrons from a beam such as inelastic scattering, capture, or fission.

The neutron, upon entering a nucleus, forms a compound state, whose excitation energy is rapidly distributed over a large number of particles. These compound states exhibit themselves in the form of resonances in the cross section curve at various energies. The field of neutron physics is concerned pri-

marily with a study of cross sections in an attempt to acquire knowledge about nuclear structure.

A transmission experiment is usually employed for the measurement of total cross sections. The experimental transmission ratio at a given neutron energy is determined by computing the ratio of neutron counts obtained when the sample to be studied is in the beam to those obtained when it is out of position. Then the total cross section is determined from the relation

$$T = e^{-N\sigma}$$

where T is the transmission, N is the number of atoms/cm^2 of the sample and σ is the total cross section at the energy in question.

The method used in this experiment is a pulsed beam time-of-flight technique similar to a system previously reported by Cranberg, Beauchamp, and Levin at the Los Alamos Scientific Laboratory.[2]

Time-of-flight techniques for measurement of neutron velocities are now well established for slow neutrons, but the development of the techniques for higher energies has only recently been accomplished. The chief reason for this delay is that the technicalities encountered in measurement of fast flight times have been overcome only in the past few years. For fast neutrons, that is, in the range 0.1 to 15 Mev, and path lengths on the order of meters, the flight times are in the range 10^{-9} to 10^{-7} seconds. Only with the recent developments in photomultipliers, scintillators, and amplifiers could such measurements be made. Thus considerable experimentation is in progress in the field of fast neutron time-of-flight spectroscopy, in particular, with regard to inelastic scattering of neutrons.

The advantages of the time-of-flight method over other types of detection systems are twofold. First, background problems are not encountered as the

background count is always taken simultaneously with the neutron count at every energy point. This is discussed in more detail in Chapter IV. Secondly, the method discriminates against neutrons of different energies so that only those of a chosen energy are counted. The Li^7 (p,n) Be^7 reaction ceases to be monoenergetic above 650 kev at which point a second group of neutrons arises from the formation of the residual nucleus Be^7 in the 430 kev excited state. This second group is observed as a peak in the spectrum which is separated in time from the main neutron peak and thus will not be counted. Previous total cross section experiments, using BF_3 counters which can not discriminate against these groups, were thus limited in the use of Li^7 (p,n) Be^7 as a neutron source.

It was decided to employ this time-of-flight method to measure the total cross section of iron as a check on previous work done by Hibdon.[3] His work was performed with a proportional counter arrangement using neutrons emitted at 120° with respect to the direction of the proton beam. The second group of neutrons from the Li^7 (p,n) Be^7 reaction first appears at a proton energy of 2.378 mev at an angle of 0° with respect to the proton beam direction. It begins to appear at 120° at a proton energy of about 2.43 Mev, at which the energy of the first group of neutrons is near 280 kev. The low energy resonances of iron might be expected to produce peaks at higher energies due to this group of low energy neutrons. This fact was taken into account by Hibdon, but the yield data on the two groups which were used were values quoted by Batchelor [4] for the 0° angle, rather than the 120° angle. Recent work at this laboratory using a time-of-flight method indicated that the yield of the low energy group is nearly isotropic at the energies under consideration, while the yield of the main group falls with increasing angle.[5]

Batchelor and Morrison [6] also showed that, in the center of mass system, the angular distribution of the low energy group is nearly isotropic for the lower proton energies. It would thus be expected that at 120° the yield ratio of the low energy group to the main group would be higher than at 0°. Therefore iron was run at 0° from 250 to 430 kev to determine if any of the resonances reported in this region could be caused by, or be contributed to, by the low energy neutron group. Also, the narrow level spacing of the resonances in the region covered would test the resolution ability of the apparatus. The peak heights and neutron widths for the observed resonances are discussed in the chapter on results.

Lead was chosen to be the second element to be investigated by this time-of-flight method. Previous measurements of the total neutron cross section of natural lead [7,8] showed the existence of three distinct maxima which were attributed to resonant interaction of neutrons with Pb^{208} to form excited states in the compound nucleus Pb^{209}. A study of these levels is of particular interest because Pb^{208} is a double closed shell nucleus consisting of 82 protons and 126 neutrons. For the heavier elements in general no resonances are observed in the fast neutron region, only smooth average cross sections. Exceptions to this trend are found only in the heavy elements lead and bismuth which, because of their "magic number" of nucleons, resemble light elements. Therefore, certain characteristics of the compound nucleus Pb^{209} can be compared with predictions of nuclear shell theories.

Since natural lead consists of the isotopes Pb^{208}, Pb^{207}, Pb^{206}, and Pb^{204} in relative abundances 52, 23, 24, and one per cent respectively, interpretation of the resonances is difficult. In the previous work,[8] measurements were taken on the total cross section of radio-lead which consists of 88 per cent Pb^{206}, nine per cent Pb^{207}, and three per cent Pb^{208}. Then the

effects of the Pb^{206} were subtracted out and, assuming that the cross section of Pb^{207} varied smoothly with energy, the contribution of Pb^{208} at the resonances was estimated.

In this experiment a different approach was used in that the natural lead cross sections were directly compensated for the effects of Pb^{206} by use of a radio-lead sample in place of the usual out count. A total cross section of uncompensated lead was taken simultaneously over the energy range covered which was 300 to 750 kev. A total cross section curve of radio-lead using that sample and the regular out count is also shown and discussed in this paper.

CHAPTER II

THEORY

The quantum mechanical theory of neutron resonance scattering is based upon the dispersion treatment of Breit and Wigner.[9,10] This theory was arrived at through an analogy between nuclear resonance processes and the theory of optical dispersion. A good discussion of the formula is given by Feshback, Peaslee, and Weisskopf [11] who gave a "derivation" based on a consideration of the wavefunction of the neutron and nucleus at the surface of the latter. A more complete treatment is found in Hlatt and Weisskopf.[1]

In the neighborhood of a resonance the expression for the cross section for elastic scattering, which is the predominant effect at our energies for nuclei that are not too light is given by:[12]

$$\sigma_{sc} = \sigma_t = 4\pi\lambda\!\!\!^{-2} \; (2l+1)\, g_J' \left| \frac{\Gamma/2}{E - E_0 + i\Gamma/2} + e^{i\delta_l} \sin\delta_l \right|^2 + P_{sc} \qquad (1)$$

$\lambda\!\!\!^{-}$ is the wavelength of the incident neutron divided by 2π, E_0 is a parameter which is very closely the energy at which σ is a maximum, Γ is the total width of the level which is nearly equal to the width of the curve at

half maximum, ℓ is the angular momentum of the incident neutron in units of $\hbar$, and g_J' is the statistical weight factor of the particular state of the compound nucleus of total angular momentum J which is responsible for the resonance. If the spin of the target nucleus is represented by I, then g_J' is given by

$$g_J' = \frac{2J+1}{2(2I+1)(2\ell+1)} \tag{2}$$

J is restricted to values $|\ell - j| \leq J \leq |\ell + j|$ where j is the so-called "channel spin".

$$j = I \pm s$$

where s is the spin of the incoming particle, which in our case is a neutron whose spin is 1/2. The combination $(2\ell+1)g_J'$ is often replaced by the symbol g_J

$$g_J = (2\ell+1)g_J' = \frac{2J+1}{2(2I+1)} \tag{3}$$

The terms $e^{i\delta_\ell} \sin \delta_\ell$ and P_{sc} arise from the potential scattering, the non-resonant portion of the scattering. The first one arises from that part of the potential scattering which has the same ℓ and J values as the resonant level and which therefore interferes coherently with the resonant scattering. The term P_{sc} represents the background of incoherent potential scattering arising from levels of different ℓ and J. It has the form

$$P_{sc} = 4\pi\lambda\!\!\!^{-2} \sum_{\ell' \neq \ell} (2\ell'+1)\sin^2\delta_{\ell'} + 4\pi\lambda\!\!\!^{-2} \ (1-g_J') \ (2\ell+1) \ \sin^2\delta_\ell \tag{4}$$

The potential scattering phase shifts δ_ℓ are given by the formula

$$\delta_\ell = - \tan^{-1} \frac{J_{\ell+1/2}(X)}{N_{\ell+1/2}(X)} \tag{5}$$

where J and N are the well known Bessel functions and x is given by

$$x = 2\pi R' / \lambda = kR' = R'/\lambda\!\!\!^{-}$$

R' is the effective nuclear radius (or scattering length) which is a parameter of the optical model.[13]

For $\ell = 0,1,2$ the explicit formulae for the phase shifts are

$$\begin{aligned} \delta_0 &= x \\ \delta_1 &= x - \pi/2 + \text{arc cot } x \\ \delta_2 &= x - \pi + \text{arc cot } \frac{x^2-3}{3x} \end{aligned} \tag{6}$$

For small x one can easily obtain the following series expansions for δ_1 and δ_2:

$$\begin{aligned} \delta_1 &= x^3/3 - x^5/5 + \ldots, && x \ll 1 \\ \delta_2 &= x^5/45 - x^7/189 + \ldots, && x < 1 \end{aligned} \tag{7}$$

Thus only the S ($\ell = 0$) potential scattering is important for x smaller than unity.

If there is no resonant scattering the S potential scattering cross section is

$$\sigma_p = 4\pi\lambda\!\!\!^{-2} \sin^2\delta_o = 4\pi R'^2 \frac{\sin^2 x}{x^2} \tag{8}$$

If x is much less than one (i.e., small phase shift) then this reduces to the usual form for the S potential scattering:

$$\sigma_p = 4\pi R'^2 \tag{9}$$

If all the δ's are small, the first term in the absolute sign of equation (1) will predominate in the vicinity of a resonance, but far from a resonance,

i.e., $|E-E_o| > \Gamma/2$, it is only the potential scattering terms which are important, and σ is given approximately by

$$\sigma = 4\pi\lambda^2 \sum_{\ell} (2\ell+1)\sin^2\delta_\ell \qquad (10)$$

If both terms in the absolute sign of equation (1) are of comparable magnitude in the neighborhood of E_o, interference can occur between the resonant and potential scattering and we observe a dip or cross section minimum preceding the resonant peak. This is observed usually only in S-wave interactions where S potential scattering is predominant. However, as will be indicated in this thesis, resonances are observed above 300 kev in the heavy nucleus lead which shows P-wave potential interference effects.

The values of E at the maxium and minimum are given by [12]

$$E_{max} = E_o + (\Gamma/2)\tan\delta$$
$$E_{min} = E_o - (\Gamma/2)\cot\delta \qquad (11)$$

At the minimum the quantity in the absolute sign in equation (1) is zero, while at the maximum the quantity has magnitude unity. Thus the maximum value of the cross section arising from a given level is

$$\sigma = 4\pi\lambda^2 g_J \qquad (12)$$

Theoretical maximum cross sections for I=o nuclei, given by the equation (1), for $\ell = 0$ and $\ell = 1$ are:

$$\sigma_{max} = 4\pi\lambda^2 \qquad \ell = 0,\ J = 1/2,\ g_J = 1$$
$$\sigma_{max} = 4\pi\lambda^2(1 + \sin^2\delta_o) \qquad \ell = 1,\ J = 1/2,\ g_J = 1 \qquad (13)$$
$$\sigma_{max} = 4\pi\lambda^2(2 + \sin^2\delta_o) \qquad \ell = 1,\ J = 3/2,\ g_J = 2$$

It is possible to obtain considerable information as to the angular momentum of the interacting neutrons by considering the level widths. The width for emission of a neutron, $\Gamma_{n,\ell}$, depends upon the magnitude of the centrifugal potential barrier. These widths may be separated into three parts:[14]

$$\Gamma_{n,\ell} = 2(1/\lambda\!\!\!^{-}) \gamma_n^{\,2} \, T \qquad (14)$$

where $\gamma_n^{\,2}$, the "reduced width", is proportional to the square of the matrix element for the transition, and depends upon the configuration of the states involved. This quantity is independent of ℓ and should not vary much from resonance to resonance. Its maximum theoretical value, called the Wigner limit, is given by[15]

$$\gamma_n^{\,2}{}_{max} = 3\hbar^2 / 2mR \qquad (15)$$

where m is the mass of the neutron and R the nuclear radius. The term $1/\lambda\!\!\!^{-}$ is proportional to the volume of phase space available to the emitted neutron and T is a centrifugal barrier penetration factor given by:

$$\begin{aligned} T_0 &= 1 \\ T_1 &= x^2/(1+x^2) \qquad\qquad x=R/\lambda\!\!\!^{-} \\ T_2 &= x^4/(9+3x^2+x^4) \end{aligned} \qquad (16)$$

Since these penetration factors are very much different for small x, the magnitude of Γ_n is an indication of the angular momentum of the neutrons which excited the level.

Since the neutron widths contain the factor $1/\lambda\!\!\!^{-}$ which is proportional to the neutron energy it is useful to convert Γ_n's to their values at 1 electron volt, this reduced neutron width (not to be confused with the pre-

ceding γ_m^2 reduced width of Wigner) being defined by:

$$\Gamma_n^o = \Gamma_n \sqrt{\frac{1\ (ev)}{E\ (ev)}} \qquad T \tag{17}$$

From the preceding relationship it is observed that for a given value of ℓ ,

$$\Gamma_n^o = b\,\gamma_m^2 \tag{18}$$

where b is a constant whose value is 4.39×10^9.

In connection with nuclear models it is more significant to discuss the <u>average</u> reduced neutron widths, $\overline{\Gamma_n^o}$, in a particular nuclide especially as it is related to the average level spacing, D, in the nuclide. The ratio $\overline{\Gamma_n^o}/D$, called the <u>strength function</u>, is especially significant with regard to the "cloudy crystal ball" model of the nucleus.[13] The neutron width of a level is an internal nuclear property for it gives the probability of disintegration of the compound state by neutron emission, but after division by the average level spacing the ratio is a measure of the penetrability of the nuclear surface.[16]

There is no known theory which will predict the energies (E_o), widths (Γ), or quantum numbers (J) of the compound states of any nucleus. The "cloudy crystal ball" model of Feshbach, Porter, and Weisskopf [13] predicts the average cross sections in terms of a model of the nucleus in which the neutron moves in a potential well, including a complex component to take account of "absorption", i.e., compound nucleus formation. The Breit-Wigner theory serves as a basis upon which the quantum numbers and widths can be determined from well resolved resonances.

CHAPTER III

EXPERIMENTAL APPARATUS

NEUTRON SOURCE

Protons from the Duke University 4 mev Van de Graaff accelerator were used to bombard lithium targets to produce the neutrons used in this experiment. The protons were analyzed by both a magnetic and an electrostatic analyzer. The magnetic analyzer deflected the proton beam 17° in the horizontal plane and separated protons from singly ionized hydrogen molecules, deuterium ions and other impurities in the beam. The proton beam strength at this point was about 25 to 50 microamperes.

Principal energy analysis was accomplished in the electrostatic analyzer[17] which deflected the proton beam through a horizontal angle of 90°. The energy distribution of the protons after passing through the analyzer is approximately triangular in shape and at half height its width was about 1 part in 800 for the iron data and 1 part in 1500 for the lead. This improved resolution results in a reduction of beam strength to about 2 to 8 microamperes at the exit of the electrostatic analyzer.

The beam, consisting of nearly monoenergetic protons was passed between two parallel plates 30 cm long separated by a distance of 0.8 cm. A 4-megacycle radio frequency voltage from a power oscillator was applied to these plates to deflect the beam across a 1/8 inch slit 8×10^6 times per second. These proton pulses, whose intensity was reduced to 1/50 or 1/100 of the steady beam strength, then bombarded a lithium target to produce "bursts" of neutrons of approximately 5 μsec duration.

Since the pulsed proton beam was only about .02 to .1 microamperes, it was decided, when taking the lead data, to employ a device developed at this laboratory by Parks, Newson, and Williamson [18] called the homogenizer. The homogenizer takes a signal from the exit slits of the analyzer and applies a voltage correction to the low potential plate of the electrostatic analyzer which keeps the beam centered through the analyzer and thus increases the beam intensity on the target. In addition to correcting the analyzer voltage, corrections are also made to the beam energy before striking the target by the application of a varying target voltage supplied by the homogenizer. It was found that a beam increase of as much as 300 per cent could be obtained by using this device.

The neutrons produced at the target were detected by an organic scintillator, details of which are discussed in a later paragraph.

A charcoal trap cooled by liquid nitrogen was used near the lithium target to improve the vacuum and help prevent the deposit of impurities on the target. A vacuum of about 0.1 micron was maintained in the vicinity of the target.

A viewing quartz located in the VSC box near the target made it possible to view the beam for alignment purposes. Also, since the quartz was insulated, it could be used to integrate the unpulsed beam and determine its strength.

The unpulsed beam could not be placed directly on the target as this would overheat the lithium coating.

The plumbing was terminated by a 6 inch section of glass pipe which served to insulate the target from the remainder of the system. The glass contained a 3 inch section of brass shim stock fitted around the inner circumference. A negative voltage from a 300 volt battery was applied to this ring to repel secondary electrons ejected from the target by the beam.

A floor plan of the entire system is illustrated in Figure 1.

The time-of-flight equipment consisted essentially of the deflection oscillator, the detector, the pulse amplifiers, the fast coincidence circuit, the time-to-pulse height converter and amplifier, and the pulse height analyzer. A photograph showing the electronics equipment is shown in Figure 2.

NEUTRON DETECTION

For total cross section measurements in the energy range considered here there are four factors upon which the counting rate depends. These are the thickness of the lithium target, the detector efficiency, the solid angle which the detector subtends at the target, and the target current. Good energy resolution requires the use of a thin target and a small solid angle of acceptance. The target current must be as large as possible to reduce the time required to take the data yet not so high as to damage the target. Since the deflection oscillator reduces the beam strength by a factor of about 1/100, every effort must be made to obtain the maximum possible beam at the output of the electrostatic analyzer. The remaining item, the detector efficiency, must be as great as possible to obtain fast counting rates.

Detectors which have been used in the past for fast neutron work include

Figure 1

FLOOR PLAN

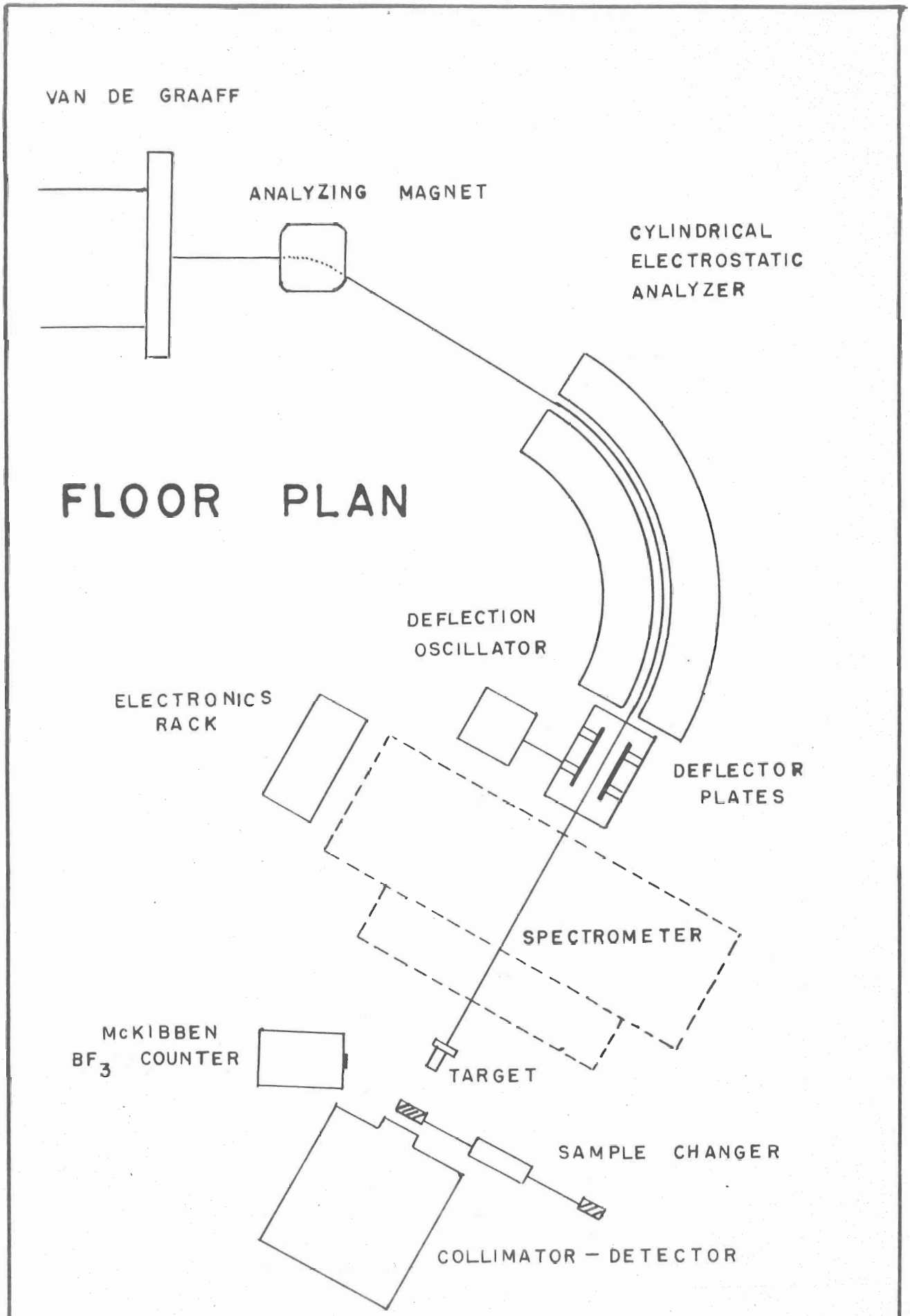
VAN DE GRAAFF
ANALYZING MAGNET
CYLINDRICAL ELECTROSTATIC ANALYZER
FLOOR PLAN
DEFLECTION OSCILLATOR
ELECTRONICS RACK
DEFLECTOR PLATES
SPECTROMETER
McKIBBEN BF_3 COUNTER
TARGET
SAMPLE CHANGER
COLLIMATOR – DETECTOR

Figure 2

PHOTOGRAPH OF THE ELECTRONICS

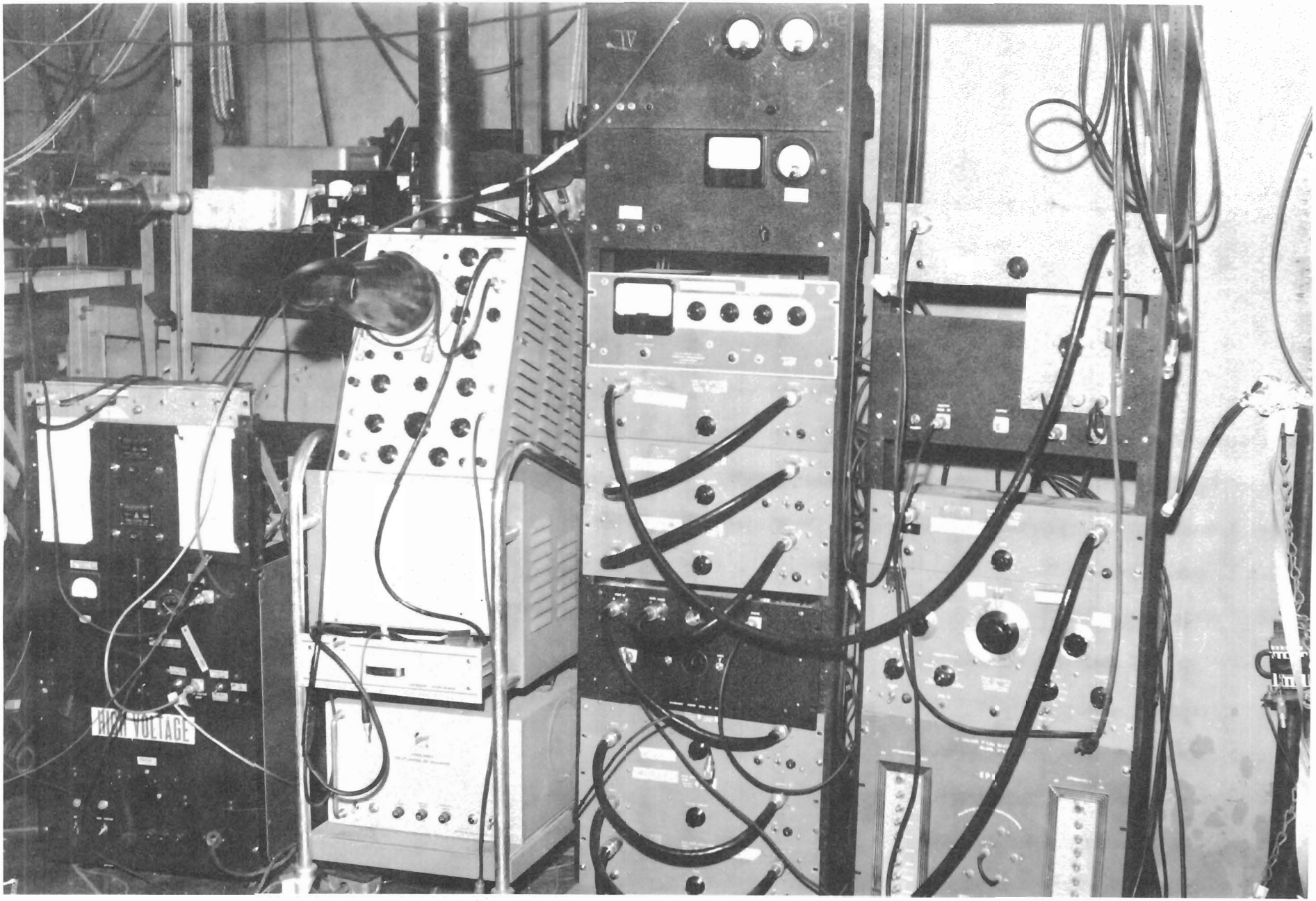
HIGH VOLTAGE

ensembles of BF_3 counters in a matrix of moderator, or proton-recoil detectors. The first type has low efficiency for fast neutrons unless it is of a large size and then shielding problems are presented. Also these counters cannot be used for measurement of total cross sections at the higher energies using the $Li^7(p,n)Be^7$ reaction as a neutron source since this reaction ceases to be monoenergetic and the BF_3 counters have no energy discrimination.

Proton recoil detectors have a high efficiency if a thick hydrogenous scintillator and a low bias can be employed. Such is the case with the time-of-flight technique discussed here. Since unwanted neutrons, such as the second group from the Li^7 (p,n) Be^7 reaction, as well as gamma rays, are discriminated against by time, they can be easily separated from the main neutron group.

The arrangement used in this experiment consisted of two RCA 6342 photomultipliers looking at a block of "Sintilon" plastic scintillator furnished by the National Radiac Corporation. The plastic was in the shape of a cylinder 2 inches thick and diameter 2 inches. Surrounding the tubes and plastic was 3/16 inch of lead to shield the counters from most of the gamma ray background. The crystal and phototubes were inserted into a large "barrel" collimator composed of 1/2 $LiCO_3$ and 1/2 paraffin (by weight). The dimensions of the collimator were 29 inches total length and 16 inches diameter with one end tapering to 6 3/4 inches diameter. A 2 5/8 inch I.D. Bakelite tube was situated along the axis of the collimator and the phototube assembly was placed perpendicular to this tube. It was necessary to use the collimator assembly in a reversed position, i.e. the narrow end was pointed away from the target, in order to obtain good geometry. The physical arrangement is illustrated in Figure 3. A photograph showing the detector barrel in position is shown in Figure 4.

Figure 3

NEUTRON COLLIMATOR AND PHOTOTUBE ASSEMBLY

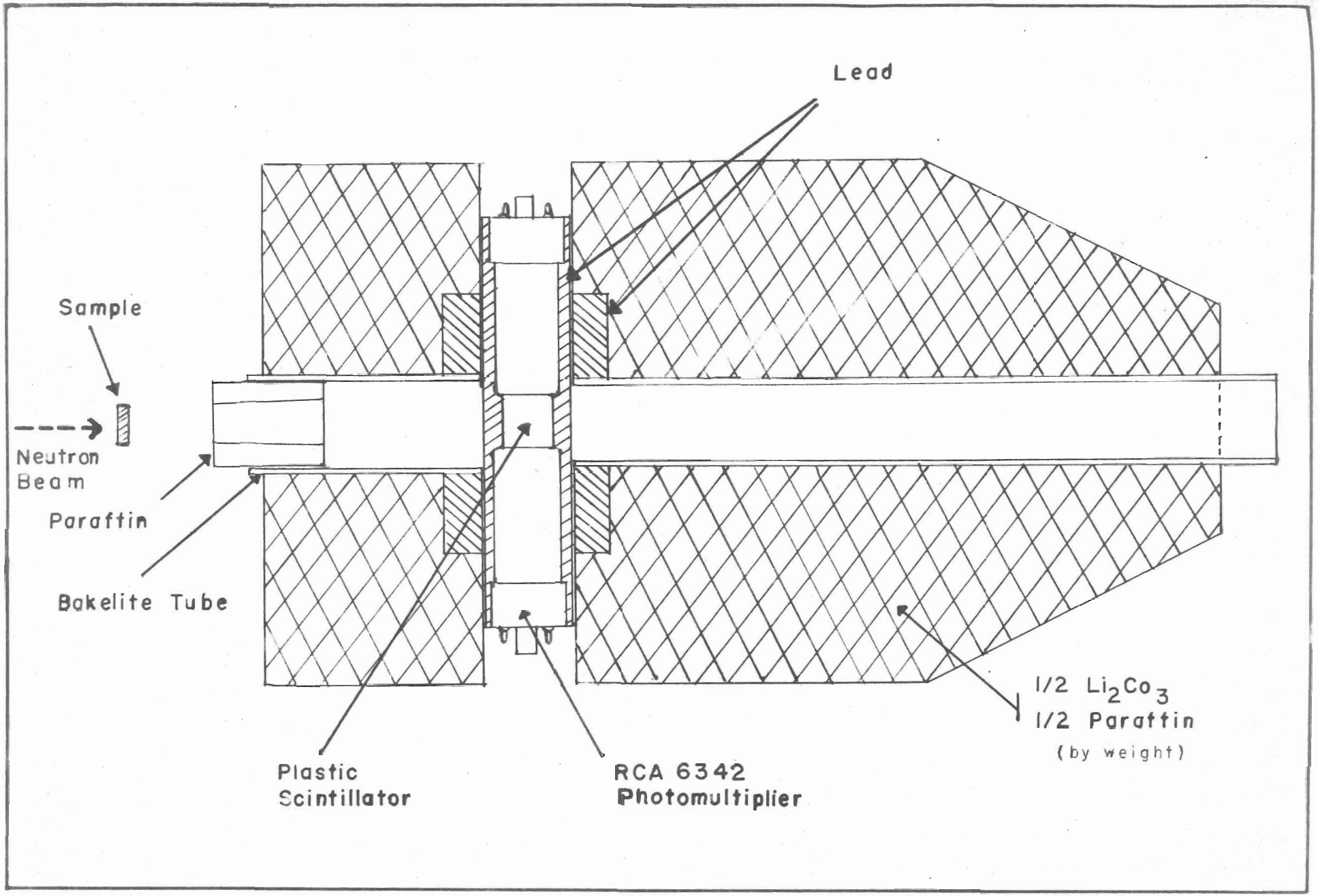
Lead
Sample
Neutron Beam
Paraffin
Bakelite Tube
Plastic Scintillator
RCA 6342 Photomultiplier
1/2 Li_2Co_3
1/2 Paraffin
(by weight)

Figure 4

GENERAL PHOTOGRAPH OF THE DETECTION SYSTEM

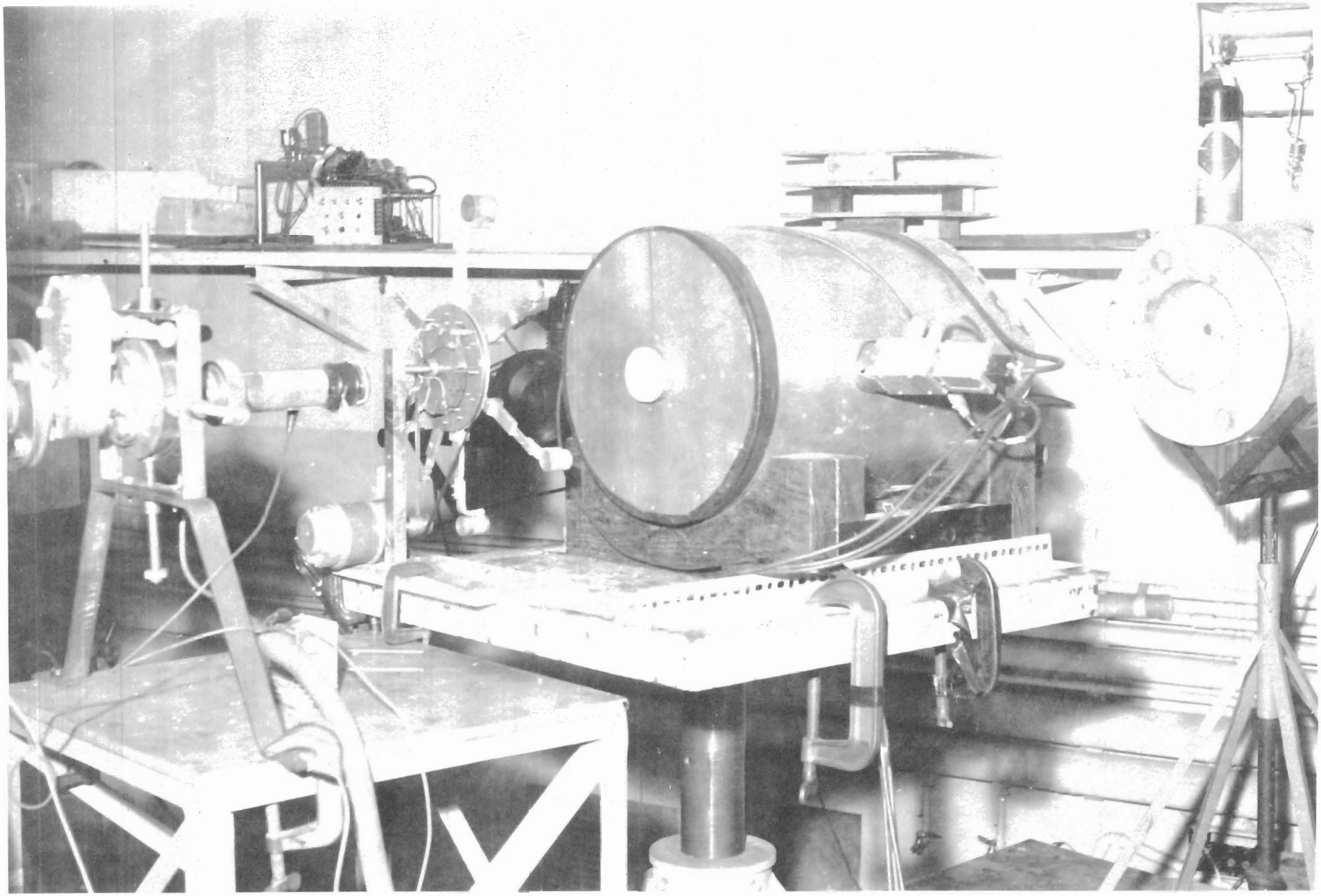

The efficiency of the detector was satisfactory down to about 250 kev due to use of the dual photomultiplier coincidence technique which considerably reduced the tube noise. Maximum counting rates were obtained at higher energies (about 400 to 500 kev) due to both increased efficiency of the detector and also to the increased yield of neutrons from the Li^7 (p,n) Be^7 reaction. The 0^0 yield from this reaction reaches a maximum at proton energy of about 2.25 mev which corresponds to a neutron energy of 516 kev. For a transmission experiment it is not necessary to know the efficiency as a function of energy as long as the efficiency has a reasonable value. This is an advantage of this type of experiment over those such as scattering in which good efficiency curves are a necessity. The detector efficiency reached a plateau at about 300 kev and its cut-off was about 150 kev. The output of the anode of each photomultiplier was connected to a plug-in cathode follower pre-amplifier whose outputs were fed to the coincidence circuit. The high voltage for the photomultipliers was 1500 - 1700 volts. At the lower neutron energies considerable increase in counting rates could be obtained by using the higher voltage but this resulted in a large number of after-pulses from which coincidences could be obtained. Since these occured at random time intervals they would tend to increase the background. Therefore a lower voltage was necessary and it was found that at 1600 volts these after-pulses were almost eliminated.

The output of each pre-amplifier was taken through a series of three Hewlett - Packard distributed amplifiers. The amplified signals were then limited by a pair of 6AH6 pentodes and fed into a biased diode fast coincidence circuit. Two signals were taken from the output, to which there was attached a short clipper. One signal was inverted by another 6AH6 and sent into the discriminator section of the time-to-pulse height converter while

the other was impressed upon a cathode follower which served as a slow gate for the pulse height analyzer.

TIME-TO-PULSE HEIGHT CONVERSION

The time-to-pulse height converter is essentially a circuit developed by Weber, Johnstone, and Cranberg.[19] The function of the converter is to convert the time interval between two pulses into a pulse whose amplitude is proportional to the interval. The interval to be measured is that between a reference signal related to the production of neutrons at the target and the signal produced by the neutron detector. Thus the flight time of the neutron between target and detector is determined.

The time of production of the neutron is inferred from the phase of the oscillating electric field through which the beam is deflected. The reference signal is taken directly from the coil across which the deflector plates are connected. This r-f voltage is fed to a circuit which generates a very short pulse for each r-f cycle and a measurement is then made of the time interval between a detector pulse (start pulse) and the next r-f pulse (the stop pulse).

The instrument is composed of three basic operational stages: a very fast acting discriminator, the converter portion, and the stop pulse shaping circuit.

The time interval of interest begins when the discriminator is triggered by a negative pulse and ends with the arrival of a stop pulse. The discriminator output is a positive square pulse whose width is determined by a section of high impedance coaxial cable (delay line). This pulse causes a saturated plate current to flow in a triode whose plate voltage drops linearly

with time, due to a 300 μμf capacitor between plate and ground. At some time during this discriminator output pulse a stop pulse will occur. This results in a coincidence which stops the linear charging of the capacitor. The output pulses of negative polarity are obtained from a cathode follower. Thus there is a linear relationship between the time interval and the final amplitude of the output pulse. The discriminator threshold dial is calibrated between zero and 100 volts but it was never necessary to operate at a setting over 15 volts. The complete circuit description and operation can be found in reference 19.

PULSE - HEIGHT ANALYSIS

The converter amplifier furnished a pulse height spectrum which is analyzed with the use of a ten-channel pulse height analyzer. The neutron groups and time-correlated gamma rays are separated in time and thus can be identified. Since there are two bursts of neutrons for every r-f cycle a double spectrum is presented, with either both complete or one complete and one incomplete depending on the symmetrization of the beam through the deflecting plates. One presentation of the double spectrum corresponds to 250 μsec. A typical time spectrum showing the neutron and gamma peaks is shown in Figure 5.

The gate signal from the fast coincidence circuit was amplified by a type "A-1" pulse amplifier and was used to gate the ten-channel analyzer. The converter output pulse was delayed approximately 0.1 μsec to insure that it arrived at the analyzer after the gate pulse whose duration was about 4 μsec. This converter pulse was then amplified by another type "A-1" amplifier before entering the analyzer. The input signal to the ten-channel analyzer

Figure 5

A TYPICAL TIME-OF-FLIGHT SPECTRUM

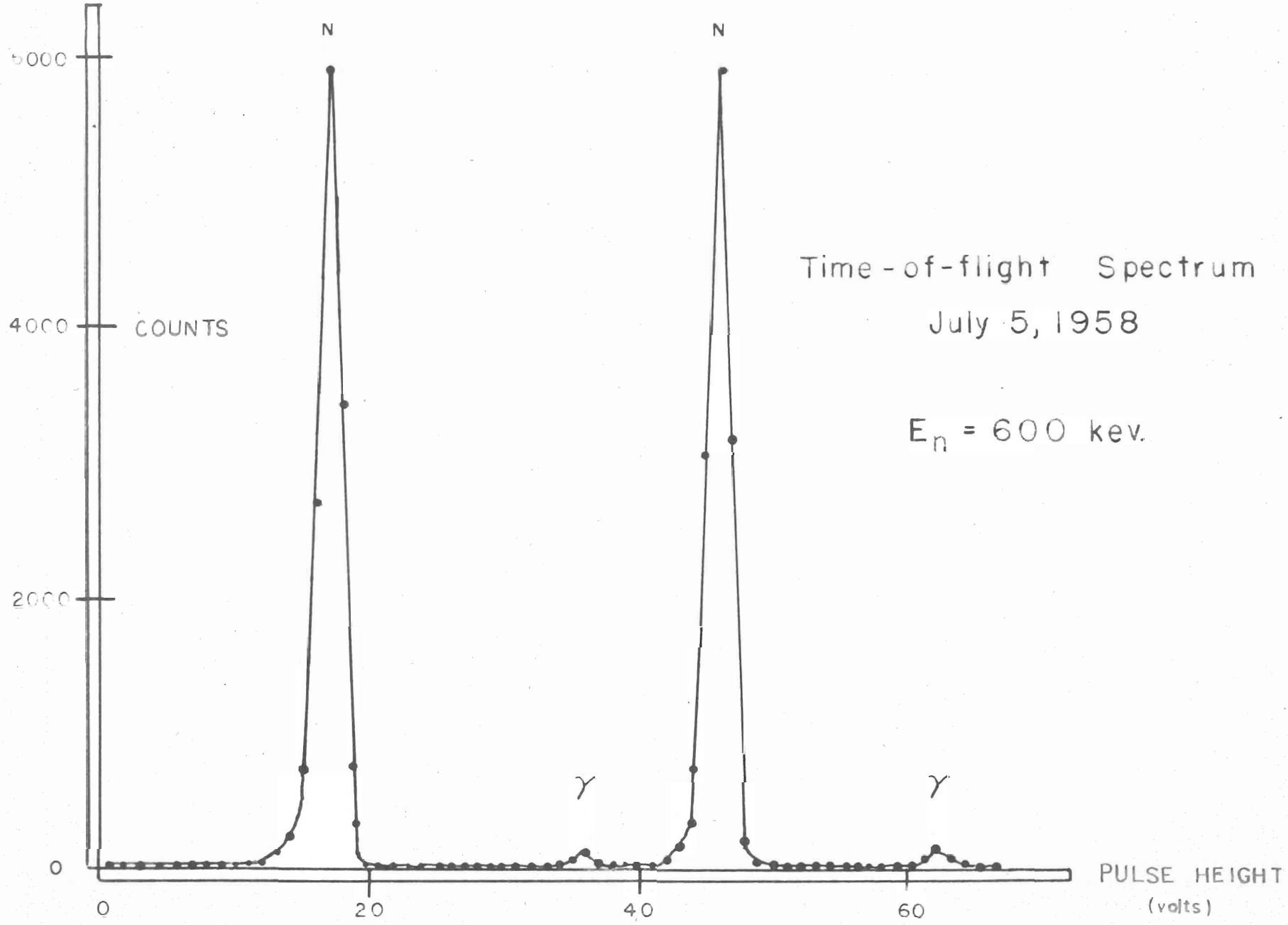
N
N
6000
4000
2000
0
COUNTS
γ
γ
0
20
40
60
PULSE HEIGHT
(volts)
Time-of-flight Spectrum
July 5, 1958
E_n = 600 kev.

was of positive polarity, about 70 volts maximum peak height, about 3 μsec pulse width (exponential decay), and a rise time of 1/2 μsec. The maximum peak height was determined by the amplifier gain which was set so as to prevent overloading.

The ten-channel analyzer could be set for either one, two, or five volt window widths. The base line bias was continuously variable from two to one hundred volts.

A view of the console showing the ten-channel analyzer is shown in Figure 6.

NEUTRON MONITORING

A McKibben type BF_3 counter [20] was placed at an angle of 60° from the axis of the beam at a distance of about 2 feet from the target to monitor the neutrons from the lithium. For every 1000 counts a pulse was sent from the glow tube scaler to the scale of 64 which in turn controlled the integrator relay. An a.c. gate on the integrator started and stopped the counting of the ten-channel analyzer. It was found that this method was preferable to integrating the beam on the target as a method of determining counting time. Any motion of the beam on an uneven lithium target would result in variations in neutron flux which would not be accounted for by integrating the beam. On the second run when the lead data was taken, the monitor was necessary as target integration could not be performed when the homogenizer was used with its high voltage target lead connected.

The pulses from the McKibben counter were amplified before entering a single channel pulse height selector set to discriminate against gamma rays.

When taking a threshold and target thickness measurement it was necess-

Figure 6

PHOTOGRAPH OF CONSOLE SHOWING TEN-CHANNEL ANALYZER

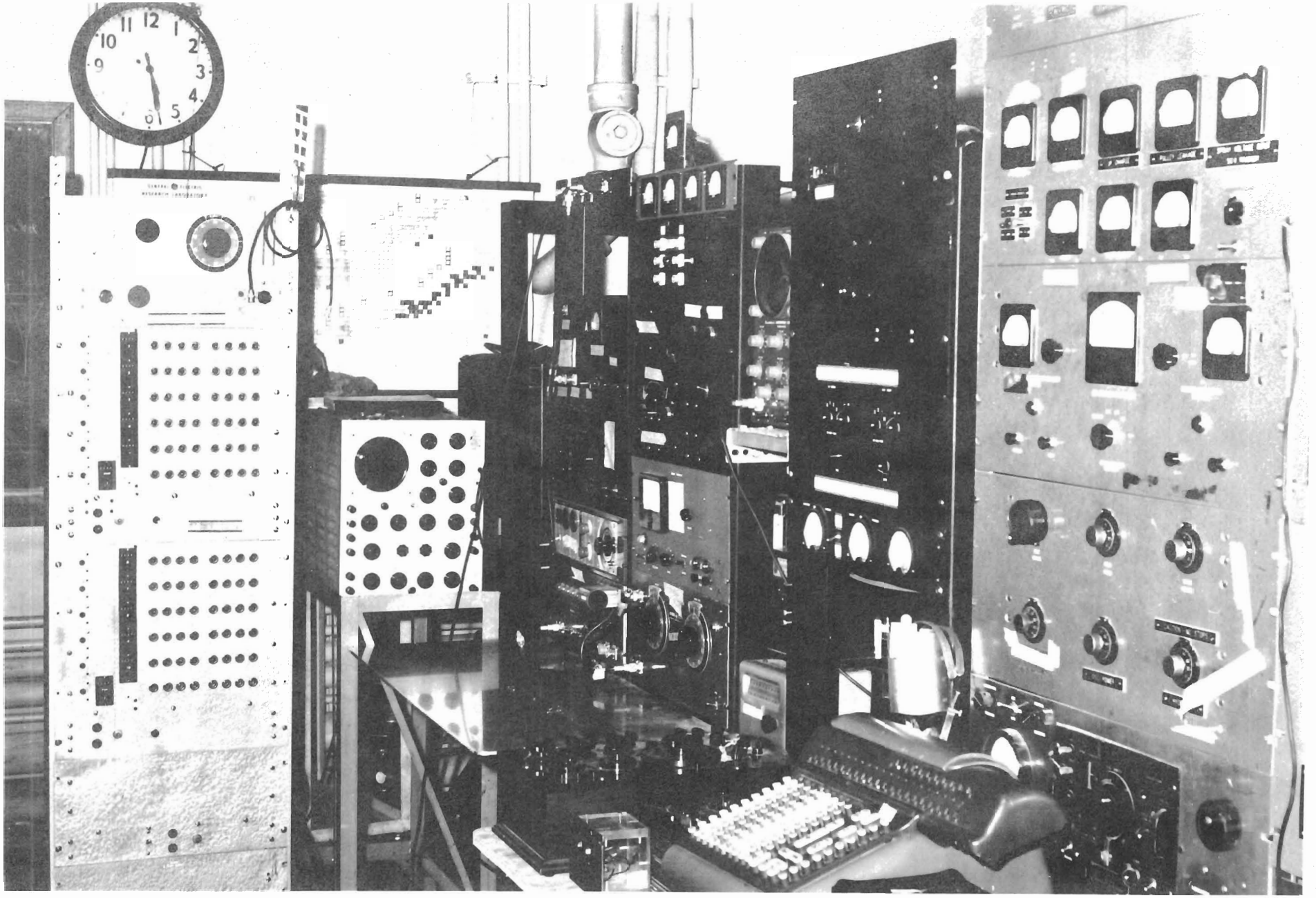

ary to remove the homogenizer and to integrate the beam on the target. This necessitated a single connector change; the scale of 64 input was switched from the glow tube scaler to the integrator scaler input.

A block diagram of the complete electronics arrangement is shown in Figure 7.

TARGETS

Lithium metal was evaporated under vacuum onto target end caps. For the iron run the caps were nickel cylinders with one end closed, about 2 inches long and 1 inch in diameter soldered to a brass flange, while for the lead run, 2 inch diameter 5 mil tantalum caps were used. After evaporation, the target was immediately removed from the evaporator and quickly mounted in position so that the lithium was not exposed to the air for more than about one minute. The caps fitted over the end of the glass pipe which terminated the beam plumbing. They were held in place by the vacuum of the system and a seal was maintained by use of an "O" ring.

Target thicknesses were measured by the familiar rise method[21] by use of the McKibben counter placed about 60 inches from the neutron source and at an angle of 0^{o} with respect to the direction of the proton beam. Although this method is valid for thick targets, it is inaccurate for very thin ones. The latter can be determined by comparing their yield to that of a measured thicker target, since the yield is approximately proportional to thickness for the target thicknesses used. The thicknesses are measured in terms of proton stopping power in the target. Targets of about 2 kev thickness were used for both the iron and lead data.

Figure 7

BLOCK DIAGRAM OF THE ELECTRONICS

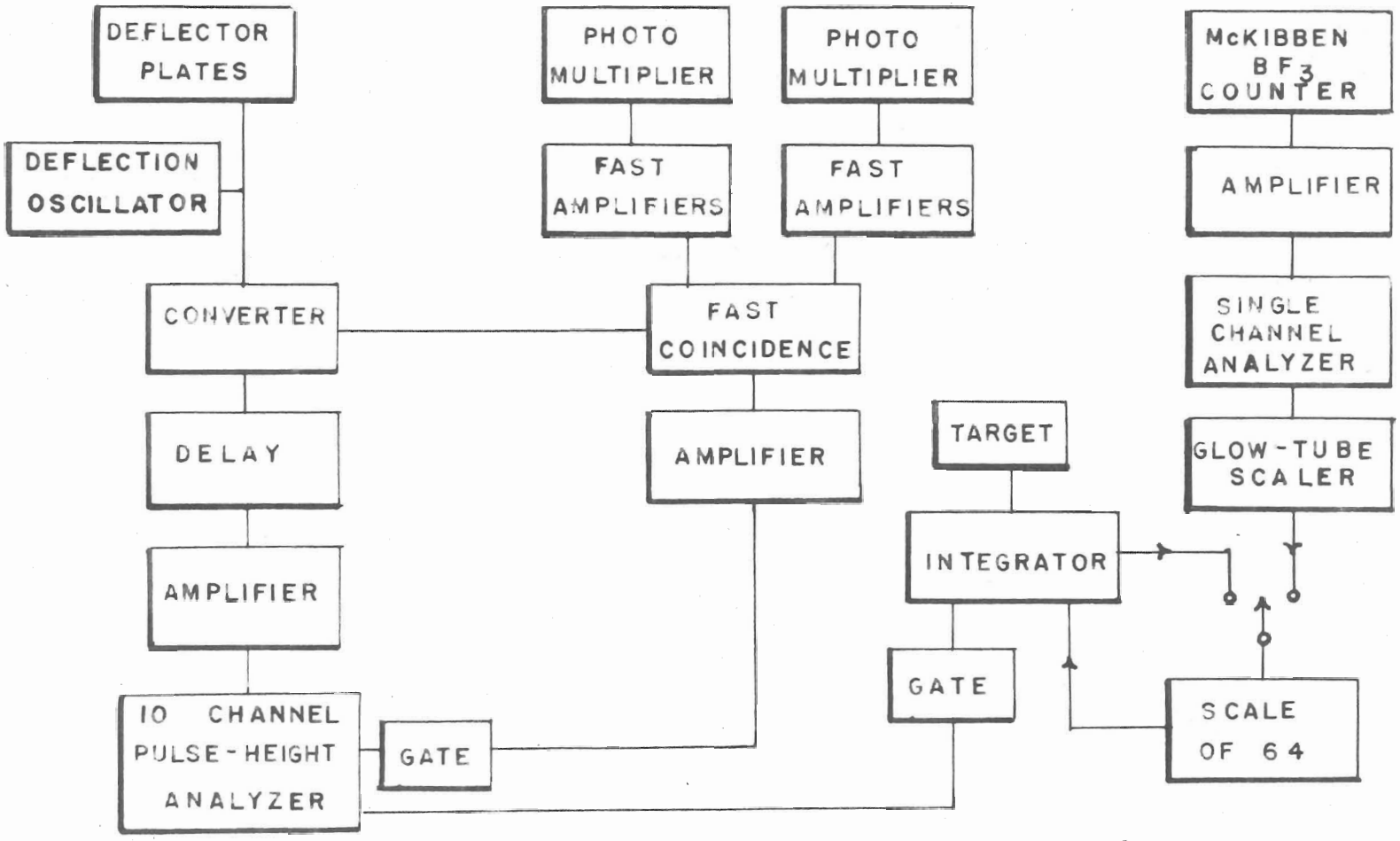
DEFLECTOR PLATES
DEFLECTION OSCILLATOR
CONVERTER
DELAY
AMPLIFIER
10 CHANNEL PULSE-HEIGHT ANALYZER
GATE
PHOTO MULTIPLIER
PHOTO MULTIPLIER
FAST AMPLIFIERS
FAST AMPLIFIERS
FAST COINCIDENCE
AMPLIFIER
McKIBBEN BF3 COUNTER
AMPLIFIER
SINGLE CHANNEL ANALYZER
GLOW-TUBE SCALER
TARGET
INTEGRATOR
GATE
SCALE OF 64

SAMPLES

The iron samples were made of Armco iron in the shape of cylinders of diameter 1.5 inches. Four sample thicknesses were used in the experiment.

The natural lead samples were poured from lead of 99.98% purity obtained from A.D. Mackay, Inc., New York. They were of 1-1/8 inch diameter. The radio-lead samples were machined to the same diameter. Sample thicknesses will be discussed in the next chapter.

The samples were mounted on aluminum spokes connected to a wheel which was rotated by a selsyn unit in order that samples could be remotely changed from the console. This arrangement was used for economy of time since the sample changer permitted the simultaneous study of several thicknesses of the same material at each energy. Also a paraffin sample mounted on the wheel could be readily introduced into the beam for spectrum check purposes. A set of indicator lights at the console showed which sample was in position. As many as eleven samples could be placed on the changer at one time. The changer was mounted such that the sample, when in place, lay midway between the target and the counter. Total target-to-counter distance was 24 inches. The samples were aligned with the axis of the collimator visually and they completely shielded the detector from the target so that no direct neutrons from the lithium could possibly be counted. The sample changer in position is shown in Figure 8.

Figure 8

PHOTOGRAPH OF THE SAMPLE CHANGER

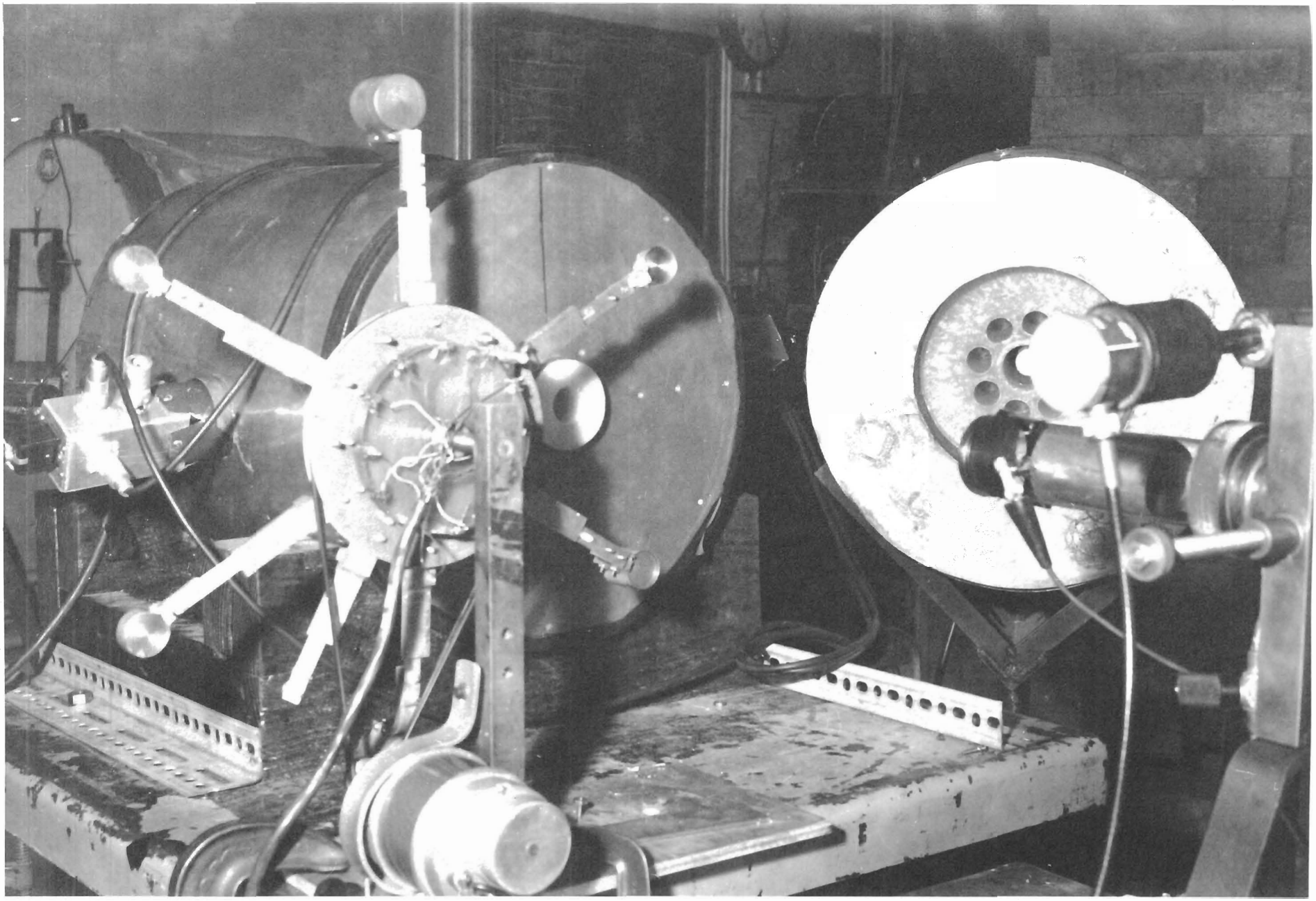

CHAPTER IV

PROCEDURE

The first step in starting a run was to check the target thickness as described previously. If the target was satisfactory, then a determination of the forward threshold of the $Li^7(p,n)Be^7$ reaction was made in order to calibrate the potentiometer on the electrostatic analyzer. Initially the value 1.881 mev[22] was used for this threshold but during the lead run the more recent value 1.8814 mev[23] was used. Once the calibration constant was determined, the Leeds and Northrup Type K potentiometer was set at the proton energy necessary to attain the desired neutron energy.

The number of neutrons was normalized by target integration for the thickness and threshold determinations. The method of normalization was then changed to the monitor as discussed in the preceding chapter.

A complete spectrum was taken using the ten-channel analyzer to determine the position of the neutron and gamma peaks. If there was any doubt as to the identification of the peaks or if an unfortunate flight path caused apparent superposition of the peaks, then paraffin or lead was inserted in the beam as a check.

If a peak occurred at the upper end of the spectrum then the electronics could smear it over the entire spectrum range resulting in an inaccurately high background. This could be corrected by interchanging the r-f cables to the deflection plates and all peaks would be shifted due to the change in phase of the stop pulse.

One of the two main neutron peaks was selected and the ten-channel analyzer bias set so as to maintain this peak within three (sometimes four) channels of two volt widths. Three (or four) other channels, separated from these and containing no neutrons or time-correlated gamma rays, contained the background counts.

At each energy point the number of counts from all ten channels were recorded, first with an empty sample holder in the beam and then with the sample in place. The sum of the three background channels was subtracted from the sum of the three "neutron" channels in each case to obtain an "out" count and an "in" count. The transmission was determined by the ratio of the "in" to the "out". The cross section could then be computed from the expression

$$\sigma = \frac{-\ln T}{N}$$

where T is the transmission, and N is the number of atoms per cm^2 in the sample. Occasionally there occurred a spectrum shift on the ten-channel analyzer due to a slight change in beam position affecting the symmetrization, and a point was retaken whenever this occurred.

At or near the resonant energy, where the cross section is high, a thin sample was used in addition to the medium thickness sample, which was used at all energies. The thinner samples were used to obtain higher counting rates and decrease the beam hardening effects, the reduction of which results in raising the experimental peak height to give better agreement with theoretical values. Away from the resonances a thick sample was used to prevent

transmission ratios near unity which cause large statistical error in the cross section.

The total cross sections of iron were measured at neutron energies of 245 kev to 425 kev. The thickness of the iron samples in grams/ cm^2 are tabulated in Table I.

The natural lead cross sections were taken by the same method as for the iron. The actual sample thicknesses were used in the calculations. In addition, a compensating sample of radio-lead was used as an out count to remove the effects of Pb^{206} on the total cross section. The thickness of each radio-lead sample was such that it contained the same number of atoms/cm^2 of Pb^{206} as a corresponding natural lead sample. The major isotopes of natural lead are Pb^{204} (1.5 %), Pb^{206} (23.6 %), Pb^{207} (22.6 %), and Pb^{208} (52.3 %). The radio-lead contains Pb^{206} (88 %), Pb^{207} (9 %), Pb^{208} (3 %). If the natural lead sample is taken with a radio-lead out count the equation for the transmission ratio is:

$$T = I_{nat} / I_{radio} = \exp\{-([N_{208} - N'_{208}]\sigma_{208} + [N_{207} - N'_{207}]\sigma_{207} + [N_{206} - N'_{206}]\sigma_{206} + N_{204}\,\sigma_{204})\}$$

where the prime refers to the number of atoms/cm^2 of the isotope in the radio-lead. If $N_{206} = N'_{206}$ then the term containing Pb^{206} vanishes leaving only the other isotopes to affect the transmission and thus the cross section. Using the compensating radio-lead sample the approximate effective composition $N_i - N'_i$ of the samples are as follows:

$\sum_i (N_i - N'_i)$

Isotope	Effective Abundance
Pb^{204}	2 %
Pb^{206}	0 %
Pb^{207}	28 %
Pb^{208}	70 %

Since a radio-lead "in" count and a regular "out" count were available, a radio-lead cross section curve was computed and graphed. These radio-lead samples, being the compensators, were thin and high transmission values were therefore obtained which can result in large statistical errors. Nevertheless, this curve is very useful and interesting in connection with the experimental results and conclusions.

TABLE I

SAMPLE THICKNESSES

Sample		Sample Thickness (atoms/ cm^2)
Iron	1/2 x	3.78×10^{22}
	1 x	8.49
	2 x	16.9
	3 x	25.5
Natural Lead	1 x	6.50
	2 x	12.7
	3 x	19.7
Radio-Lead	1 x	1.74
	2 x	3.39
	3 x	5.25
Compensated Natural Lead		Effective thickness
	1 x	4.71
	2 x	9.24
	3 x	14.3

TABLE II

ISOTOPE THICKNESSES

Sample		Isotope Pb^{208}	Pb^{207}	Pb^{206}	Pb^{204}
Nat. Lead	1 x	3.37×10^{22}	1.46×10^{22}	1.52×10^{22}	$.0966 \times 10^{22}$
	2 x	6.60	2.86	2.98	.189
	3 x	10.2	4.42	4.61	.293
Radio-Lead	1 x	.0521	.156	1.53	-
	2 x	.102	.305	2.98	-
	3 x	.157	.471	4.62	-

CHAPTER V

DATA ANALYSIS

Two general procedures, shape analysis and area analysis were employed in determining the resonance parameters.

Shape analysis uses the shape and peak height of the observed resonances as a means of determining the parameters, in particular, the ℓ and J values. The angular momentum may usually be ascertained from the distinguishing features of s-wave and p-wave resonances. The s-wave peak is asymmetric about the maximum and is generally preceded by an observable dip in the cross section, while a p-wave peak is usually symmetric. The s-wave dip is due to interference between resonance and s-wave potential scattering. At higher energies, however, where p-wave potential scattering becomes important, a dip may be observed before a p-wave peak.

A comparison of the experimental and theoretical peak heights will usually help to determine the angular momentum. The maximum value of the cross section minus the minimum value is given by

$$\sigma_{max} - \sigma_{min} = 4\pi\lambda^2 gc$$

where c is the abundance of the isotope causing the resonance. For $\ell = 0$,

σ_{min} is very nearly $(1-g_j)\,\sigma_p$. Thus for s-wave interactions with I = 0 nuclei, σ_{min} should be zero and $\sigma_{max} = 4\pi\lambda^2 gc$.

Area analysis is based on the fact that the area of a resonance on a (1-T) scale is independent of instrumental resolution providing $\Gamma/2E_o \ll 1$. [24] The area below a resonance peak on a (1-T) scale is given by

$$a = \int_o^\infty (T_p - e^{-n\sigma_t})\, dE \qquad T_p = e^{-n\sigma_p}$$

$$a = T_p \int_o^\infty (1 - e^{-n(\sigma_t - \sigma_p)})\, dE$$

The term $(\sigma_t - \sigma_p)$ is obtained from the Breit-Wigner equation. In the usual methods of area analysis, the interference term in the Breit-Wigner equation is neglected and the integral is evaluated with this approximation. The result of the integration yield

$$A' = \pi\Gamma_n(N\sigma_o/2)\, e^{-N\sigma_o/2}\left[I_o(N\sigma_o/2 + I_1(N\sigma_o/2)\right]$$

where $A' = a/T_p$, I_o and I_1 are Bessel functions of imaginary arguments, and σ_0 is the theoretical peak height of the resonance.

Curves are available in which Γ/A' is plotted against $N\sigma_o$ for various values of Doppler broadening (which is usually taken to be zero). The area is measured with a planimeter, $N\sigma_0$ assigned a value based on the g value selected, and Γ is thus determined from the curves. In measuring the area, an energy range E_1 is taken on both sides of E_o such that E_1 is greater than the level width, the Doppler width, and the instrumental resolution but much less than E_o. The area measured is between $E_o - E_1$ and $E_o + E_1$ with the area in the wings neglected in taking the measurement. This neglected area is calculated from

$$\text{Area neglected} = N\sigma_o\Gamma^2/2E_1$$

with the assumption that half the area lies on each side of the resonance. This calculated correction is added to the measured area to give the total area under the 1-T curve.

This method of area analysis was employed for the lead resonances.

Seth [25,26] has recently developed an analysis method in which the interference term in the Breit-Wigner equation is not neglected. Also he has shown that for s-wave resonances the phase relation between resonance and potential scattering amplitudes, which is usually neglected, should be retained. Furthermore, he has employed an IBM 650 computer to perform numerical integrations of area between finite limits around E_o, namely 2, 5, 10, and 20 Γ's. Thus resonances which are poorly defined because of very close neighboring resonances can be analyzed to a much higher accuracy than could be done previously. An outline of this procedure is given here.

The Breit-Wigner equation for resonance scattering may be written in the form

$$\sigma_t - \sigma_p = \frac{\sigma_o}{1 + X^2} \left[\cos 2\alpha + x \sin 2\alpha \right]$$

where $\sigma_o = 4\pi \lambda^2 g \, \Gamma_n / \Gamma$

$\alpha = R' / \lambda$

$x = 2 (E - E_o)/\Gamma \qquad dE = dx \, \Gamma/2$

Let $= \sigma_o / 1 + x^2$

$$a = T_p \int_0^\infty (1 - e^{-n(\sigma_t - \sigma_p)}) \, dE = T_p \int_0^\infty (1 - e^{-n\beta(\cos 2\alpha + \sin 2\alpha)}) dE$$

$$= T_p \, \Gamma/2 \int_{-\frac{2E_o}{\Gamma}}^\infty (1 - e^{-n\beta(\cos 2\alpha + \sin 2\alpha)}) dx$$

The lower limit may be replaced by $-\infty$ since $\Gamma \ll 2E_0$ and negligible area is included by extension of lower limit to $-\infty$.

$$a = T_p \Gamma/2 \int_{-\infty}^{\infty} (1 - e^{-n\rho(\cos 2\alpha + x \sin 2\alpha)})dx$$

$$\left(\frac{a}{T_p}\right)\frac{2}{\Gamma} = \int_0^{\infty} (1-e^{-n\rho(\cos 2\alpha + x \sin 2\alpha)})dx + \int_{-\infty}^{0} (1-e^{-n\rho(\cos 2\alpha + x \sin 2\alpha)})dx$$

If we change x to $-x$ we have

$$\left(\frac{a}{T_p}\right)\frac{2}{\Gamma} = \int_0^{\infty} (1-e^{-n\rho(\cos 2\alpha + x \sin 2\alpha)})dx + \int_0^{\infty} (1-e^{-n\rho(\cos 2\alpha - x \sin 2\alpha)})dx$$

There are two types of resonances which must be considered:

(1) Those resonances in which the area in the interference dip beneath the base line is small compared to the area under the peak on the 1-T scale. The areas are added to obtain the total area with the area beneath the base line considered negative.

(2) Those resonances in which the interference dip is comparable in size to the peak such that the algebraic addition of areas yields total area which is almost zero or even negative, in which case analysis is impossible.

The second type of resonance may be analyzed if the negative area is subtracted to obtain the total area which is characteristic of the resonance and which is not negative or near zero. The total area determined by algebraic addition of area above and below the potential scattering base line will be denoted by a_+, while that area determined by algebraic subtraction will be called a_-.

$$\left(\frac{a+}{T_p}\right)\frac{2}{\Gamma} = \int_0^\infty (1-e^{-n\beta(\cos 2\alpha + x\sin 2\alpha)})dx + \int_0^\infty (1-e^{-n\beta(\cos 2\alpha - x\sin 2\alpha)})dx$$

$$\left(\frac{a-}{T_p}\right)\frac{2}{\Gamma} = \int_0^\infty (1-e^{-n\beta(\cos 2\alpha + x\sin 2\alpha)})dx - \int_0^\infty (1-e^{-n\beta(\cos 2\alpha - x\sin 2\alpha)})dx$$

Let $a+/T_p = A+$

$a-/T_p = A-$

If we combine and rearrange terms we can obtain

$$\left[\frac{A+}{\Gamma}\right]_0^\infty = \int_0^\infty \left[1 - e^{-n\beta\cos 2\alpha}\cosh(-n\beta x\sin 2\alpha)\right] dx$$

$$\left[\frac{A-}{\Gamma}\right]_0^\infty = -\int_0^\infty \left[e^{-n\beta\cos 2\alpha}\sinh(-n\beta x\sin 2\alpha)\right] dx$$

These are the quantities which have been evaluated numerically. In addition to the evaluation between limits 0 to ∞, they have also been evaluated for finite limits 2, 5, 10, and 20 Γ. These curves between finite limits are used when it is not possible to measure the area over the entire resonance due to the interference of neighboring levels.

Graphs are plotted of $A+/\Gamma$ vs. $n\sigma_o$, $\Gamma/A+$ vs. $n\sigma_o$, and $\Gamma/A-$ vs. $n\sigma_o$ with the dimensionless quantity $(ng)^{1/2}R'$ used as a parameter. In using the graphs for the type (1) resonance, one chooses the appropriate n, g, and R', and with the measured area obtains an initial value of Γ from the $A+/\Gamma$ curves. With this initial value of Γ one uses the curves of $\Gamma/A+$, evaluated at the finite limits suitable to the particular resonance, and the new area measured between these limits to obtain a more accurate value of Γ. For the type (2) resonance, a similar procedure is executed using the $\Gamma/A-$ curves.

In measuring the area, an energy range E_1 is taken on both sides of the resonant energy E_o such that $2E_1$ is consistent with the integration limits of the curve that is used (e.g., 5Γ).

In this experiment the Γ/A- curves were used for the iron analysis since the interference dips were comparable in size to the peaks.

CHAPTER VI

EXPERIMENTAL RESULTS

The results of these experiments are shown graphically in Figure 9 through Figure 12. Experimental cross sections, in barns, are plotted against neutron energies in kilovolts. The experiment involving natural iron was performed during the period April 20 to May 1, 1958, while the lead experiments were performed during the period June 30 to July 10, 1958.

The error bars on data in this thesis represent the statistical error of the cross section as computed from the transmission standard deviation. If $\pm \Delta T$ are the limits upon the measured transmission value T, such that there is a 68 % probability that the measured value occurs within $\pm \Delta T$ of the exact value T_o (that could only be obtained by infinite counting time), then ΔT is given by[27]

$$\Delta T = (I/I_o) = \left[1/I + 1/I_o\right]^{1/2} (I/I_o)$$

where I is the "in" count and I_o is the "out" count. In terms of cross section we have

$$\Delta \sigma = 1/N \left[1/I + 1/I_o\right]^{1/2}$$

Figure 9

CROSS SECTION CURVE FOR NATURAL IRON

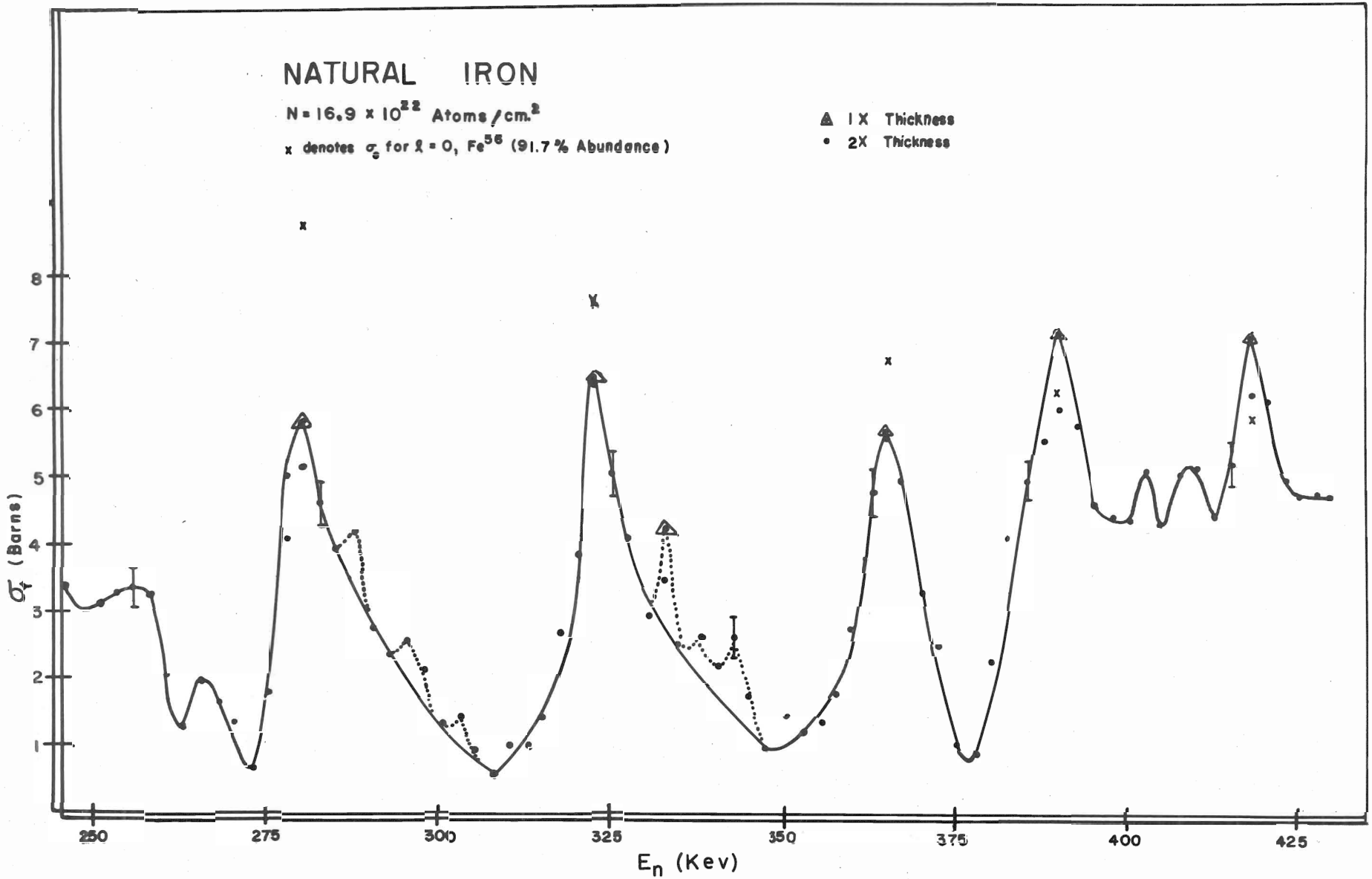
NATURAL IRON
N = 16.9 x 10^22 Atoms / cm.^2
x denotes σe for ℓ = 0, Fe^56 (91.7 % Abundance)
1 X Thickness
2X Thickness
σt (Barns)
En (Kev)
250
275
300
325
350
375
400
425
1
2
3
4
5
6
7
8

IRON

A 2 kev lithium target was used for the iron data with the electrostatic analyzer set for a proton beam spread of 1 part in 800, i.e. if a triangular distribution is assumed, the width at half-height divided by the energy is in the ratio 1/800. The total effective neutron resolution was 3 kev for the iron run.

Iron exhibits prominent resonances at 280, 323, 365, 390, and 418 kev in the energy region between 245 and 425 kev. These energies are tabulated in Table III along with the observed maxima, σ_{max}, of the cross section peaks and the corresponding theoretical maxima. Also shown are the values of the level widths, Γ_n, as determined by the improved area analysis method described in Chapter V, as well as the values of the reduced widths, Γ_n^o.

There is also evidence of levels at 265, 288, 295, 333, 343, 403, and 410 kev. No attempt was made to analyze these resonances as they are of doubtful validity and are very poorly defined. They are due to the minor isotopes of iron which are present in the natural iron sample.

The five prominent resonances are all attributed to neutron interactions with Fe^{56} (91.7 % abundance). The resonances at 280, 323, and 365 kev are all lower than $4\pi \lambda^2 c$ and are attributed to s-wave ($\ell = 0$) interactions. On the low energy side of each resonance, with the exception of the one at 418 kev, there is a deep minimum which indicates that the resonances are s-wave.

At 390 kev the thin sample cross section exceeded the calculated σ_{max} for $\ell = 0$ but the cross section of the medium thickness sample was lower. The deep minimum of 0.75 barns makes it appear certain that it is a well

resolved s-wave resonance and that the high point which is beyond statistics, is in error. Furthermore, the excellent resolution is justified since the width of this resonance is 4 kev, which is wider than the others, and the resonance should be the best resolved.

Both the thick and thin sample cross sections at 418 kev exceeded σ_{max} (cal.) for s-wave interactions. Therefore, this resonance may be a p-wave resonance with g = 1. In this case σ_{max} (cal.) = 8.83 barns where the potential scattering is included. Area analysis was not possible on this peak since it is very poorly defined. Several small peaks contribute to the high cross section between the 390 and 418 kev resonances.

A value of potential scattering was required for the analysis of the iron resonances. Since this value could not be obtained directly from the data, it was computed using the value of R' = 5.5 fermis which was obtained from low energy data taken at this laboratory.[28] The potential scattering decreased from 3.34 barns at 280 kev to 3.14 barns at 390 kev.

The level width values of 2.0, 3.5, 3.3, and 4.0 kev for the 280, 323, 365, and 390 kev resonances respectively are in excellent agreement with the values quoted by Hibdon[3] of 2.0, 4.0, 3.0, and 5.0 kev for the four resonances.

From the reduced neutron widths shown in Table III, one obtains a value of the strength function $\overline{\Gamma}^{n}_{o}/D$ of 2.0×10^{-4} for Fe^{56}. The strength function is expected[13] to reach a maximum near A= 55. The experimental value of the strength function of Fe^{56} is probably accurate to no better than 100 % as only four resonances were used in the determination. The theoretical calculations of the strength function for A = 56 vary from about 2×10^{-4} to 8×10^{-4} depending upon the optical model parameters employed.

Since Hibdon's data was taken at an angle of 120°, it is possible to

TABLE III

PARAMETERS OF THE RESONANCES IN IRON

E_n kev	ℓ	g	σ_{max} (obs.) barns	σ_{max} (cal.) barns	Γ_n kev	Γ_n^o kev
280	0	1	5.84	8.52	2.0 ± 0.5	0.38×10^{-2}
323	0	1	6.46	7.40	3.5 ± 0.7	0.62×10^{-2}
365	0	1	5.73	6.54	3.3 ± 0.6	0.55×10^{-2}
390	0	1	7.31	6.12	4.0 ± 1.0	0.64×10^{-2}
418	0	1	7.14	5.72	-	-
	1	2	7.14	8.83	-	-

have peaks at the higher energies due to the low energy group of neutrons. This has been discussed in Chapter I. It appears that the small resonances observed by Hibdon in the region under consideration are due to the main neutron group, rather than the low energy group, since they appear in the cross section curve shown in Figure 9. Since the data shown here was taken at 0^{o} and since the energies were below the threshold for the second neutron group, all resonances are due to the main group.

LEAD

The cross section curve for natural lead is shown in Figure 10, and the curve for compensated lead is shown in Figure 11.

The effective neutron resolution was about 2 kev for the lead data using a 1 kev target and the electrostatic analyzer set for a proton beam spread of 1 part in 2000.

Three distinct maxima were observed in the natural lead cross section which are attributed to resonant interactions of neutrons with Pb^{208} to form excited states of the compound nucleus Pb^{209}. The resonances occur at neutron energies of 353, 528, and 720 kev. The various parameters and experimental peak heights for these resonances are tabulated in Table IV.

The use of the compensating sample in place of the regular out count tended to raise all peak heights and lower the interference dip before the two higher energy peaks. This is expected since the effective composition of Pb^{208} is increased from 52 % to 70 % by the use of the compensator.

If the peaks were perfectly resolved then the peak height, measured from the minimum to the maximum of the cross section should be equal to

Figure 10

CROSS SECTION CURVE FOR NATURAL LEAD

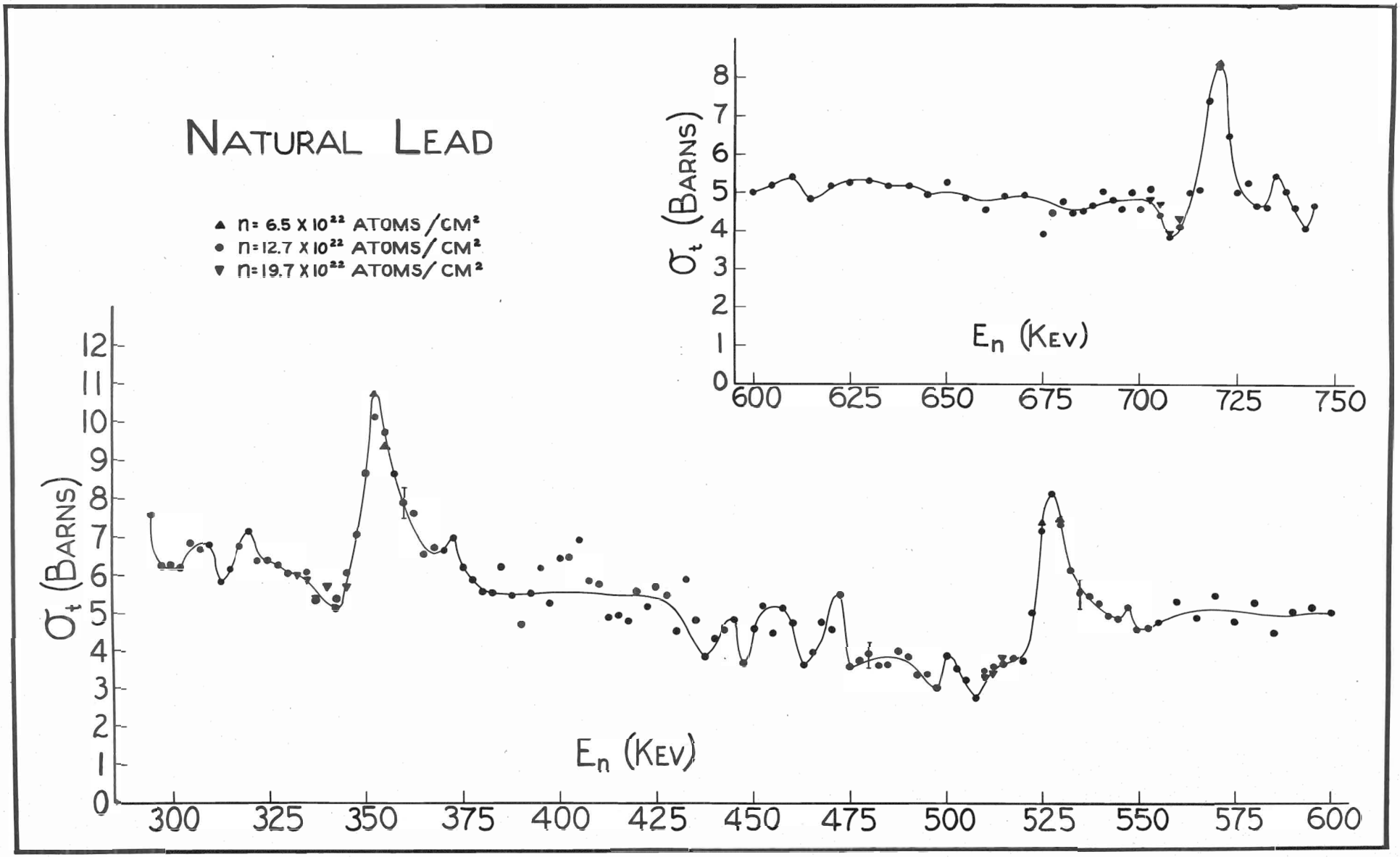
NATURAL LEAD
▲ n = 6.5 X 10²² ATOMS / CM²
● n = 12.7 X 10²² ATOMS / CM²
▼ n = 19.7 X 10²² ATOMS / CM²
σt (BARNS)
En (KEV)
0
1
2
3
4
5
6
7
8
9
10
11
12
300
325
350
375
400
425
450
475
500
525
550
575
600
σt (BARNS)
En (KEV)
0
1
2
3
4
5
6
7
8
600
625
650
675
700
725
750

Figure 11

CROSS SECTION CURVE FOR COMPENSATED LEAD

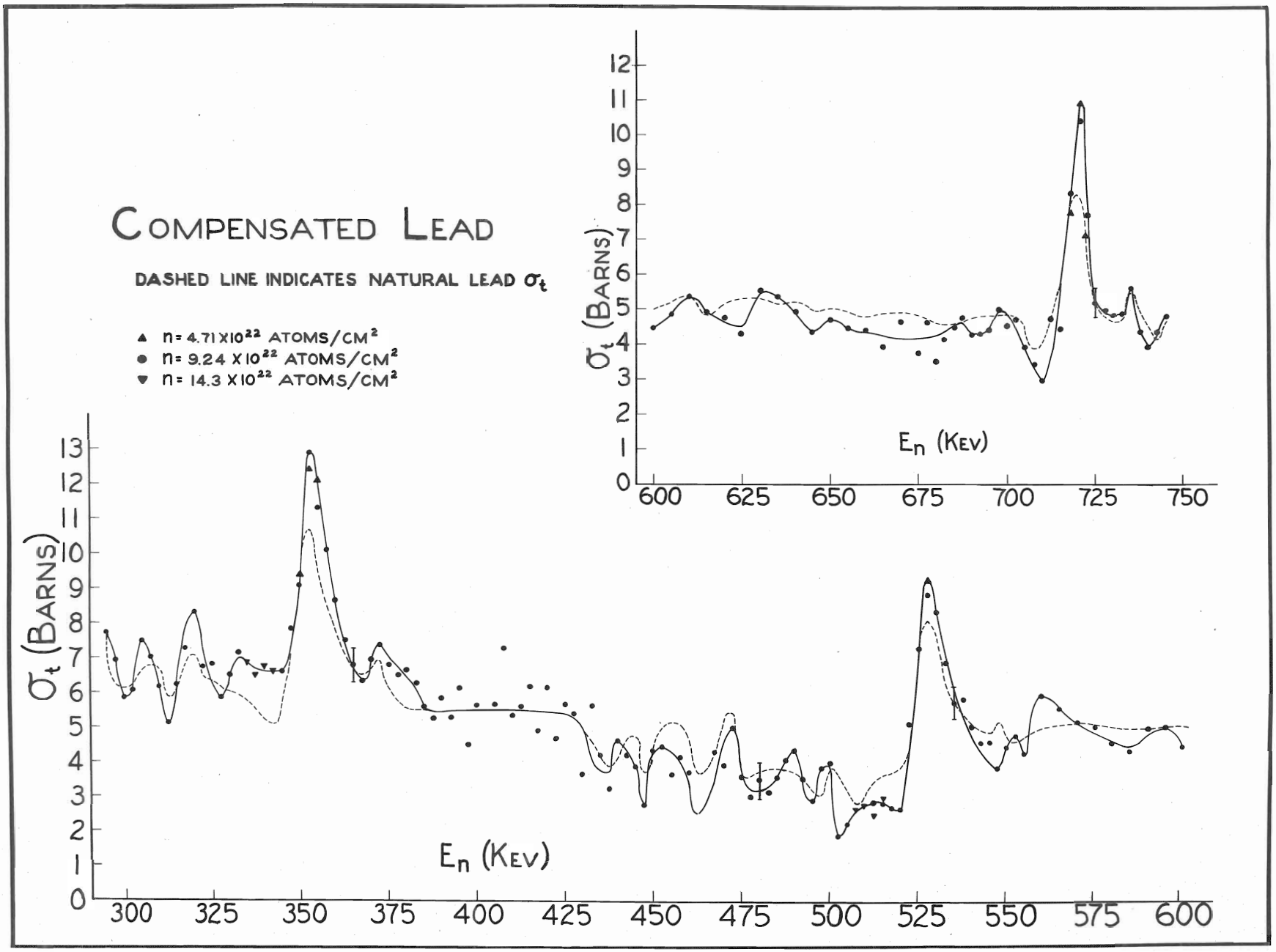
COMPENSATED LEAD
DASHED LINE INDICATES NATURAL LEAD σ_t
▲ n = 4.71 X 10^22 ATOMS/CM^2
● n = 9.24 X 10^22 ATOMS/CM^2
▼ n = 14.3 X 10^22 ATOMS/CM^2
σ_t (BARNS)
E_n (KEV)
0 1 2 3 4 5 6 7 8 9 10 11 12 13
300 325 350 375 400 425 450 475 500 525 550 575 600
σ_t (BARNS)
E_n (KEV)
0 1 2 3 4 5 6 7 8 9 10 11 12
600 625 650 675 700 725 750

$4\pi\lambda^2 gc$ where c is the relative abundance of the isotope responsible for the resonance. The energy spread for the lead experiments was about 2 kev and the analysis indicates that the level widths of the resonances are near this value, so one would not expect perfect resolution of the resonances.

For the 353 kev resonance in natural lead, $\sigma_{max} - \sigma_{min}$ is 5.6 barns which exceeds the value calculated for g = 1 but is less than the value calculated for g = 2. The compensated lead at this energy shows a difference of 6.3 barns which also exceeds the value for g = 1 but is less than that for g = 2. Therefore, this appears to be a p-wave resonance with g = 2, and the dip preceding the resonance exhibits p-wave interference effects. However, at this energy, p-wave potential scattering is only about 20 % of the total potential scattering and a large dip would not be expected. With the compensating sample the dip was nearly eliminated. Peterson et al.[8] agree with the value of ℓ = 1 but assign g = 1 rather than g = 2 for the 353 kev resonance.

The height of the peak at 528 kev, in both the natural and compensated samples, is consistent with ℓ = 1 and g = 2. The p-wave interference dip is again observed, and at this energy p-wave potential scattering constitutes about 35 % of the total potential scattering. These assignments agree with Peterson.

At 720 kev the experimental value of $\sigma_{max} - \sigma_{min}$ is 4.5 barns for the natural lead compared to calculated values 1.9 barns for g = 1, 3.8 barns for g = 2, and 5.7 barns for g = 3. For d-wave neutrons, J has values 3/2 and 5/2 and therefore g has corresponding values 2 and 3. The compensated lead shows an 8 barn difference as compared to the slightly lower calculated value of 7.6 barns for g = 3. Therefore, these peak heights indicate a d-wave interaction for this resonance. However, the interference dip is very pro-

TABLE IV

PARAMETERS OF THE RESONANCES IN LEAD

	E_n kev	ℓ	g	σ_{max} (obs.) barns	σ_{max}- σ_{min} (obs.) barns	σ_{max}- σ_{min} (cal.) barns	Γ_n kev
Nat. Lead	353	1	2	10.7	5.6	7.7	3.0 ± 0.8
	528	1	2	8.1	4.6	5.2	1.5 ± 0.5
	720	1	2	8.3	4.5	3.8	4.2 ± 0.8
		2	3	8.3	4.5	5.7	2.8 ± 0.6
Comp. Lead	353	1	2	12.9	6.3	10.5	-
	528	1	2	9.2	6.7	7.0	-
	720	1	2	11.0	8.0	5.0	-
		2	3	11.0	8.0	7.6	-

minent, in particular, with the compensating sample. The d-wave potential scattering is only about 3 % of the total as compared to about 45 % for p-wave potential scattering at 720 kev. If this is a p-wave resonance, the peak height may be explained by the incoherent addition of this resonance with another, possibly one of the other lead isotopes. Peterson assigned the values $\ell = 1$, $g = 2$ for this resonance.

The natural widths of the levels in natural lead were determined by the area analysis method of Seidl et al.[12] as discussed in Chapter V. The values obtained are lower than those quoted by Peterson et al.[12] of 8.4, 5.6, and 5.7 kev for the 353, 528, and 720 kev resonances respectively.

If the scattering of a neutron by a closed shell nucleus such as Pb^{208} could be treated as a single particle interaction, the reduced widths, γ^2, of the levels would be expected to approach the Wigner limit, γ^2_{max}. (See Chapter II). The reduced widths of the 353, 528, and 720 kev resonances are found to be about 22, 10, and 8 x 10^{-13} kev-cm respectively for p-wave interactions. The reduced width of the 720 kev resonance for d-neutrons is 2 x 10^{-13} kev-cm. The ratio of these reduced widths to γ^2_{max} are .029, .013, .01, and .003 respectively. In view of this it is concluded that the observed levels in the compound nucleus Pb^{209} are connected with many-particle excitation and are not the single-particle levels predicted by nuclear shell theory.

A number of small resonances appear in the cross section of lead. Two of these, at 308 and 320 kev, are probably s-wave resonances in Pb^{208} as their peak height increases by about one barn when the compensating sample is used. Several resonances which appear to be real are observed between 435 and 505 kev. These are levels in Pb^{206} or Pb^{207} as their heights are lower in the compensated lead cross section. Other unresolved levels of

these isotopes are indicated by the point scatter in the region 375 to 425 kev.

The cross section of radio-lead using a normal out count is shown in Figure 12. Radio-lead is 88 % Pb^{206} so the large resonances should be due to this isotope. It is noted that many of the resonances produce minima in the cross section and have an "inverted" form, i.e., appear as dips in a background of potential scattering. This behavior may be understood in terms of the phase shifts for potential scattering for s-neutrons. If the phase shift is very near $\pi/2$, there is no maximum whatsoever for resonant scattering in the Breit-Wigner equation. The cross section is almost zero at $E = E_r$ and rises on both sides of E_r to the value $4\pi\lambda^2 g$ for $|E - E_r| > \Gamma/2$. The resulting curve is that of an inverted maximum. Taking the nuclear radius of lead as 9×10^{-13} cm, the s-wave phase shift for 450 kev neutrons is about 1.3 radians. Since p-wave potential scattering is small at this energy, the minima observed at 343, 388, 395, 420, 445, 503, and 533 kev are believed to be produced by s-neutrons. The residual cross section of about one barn at the minima is due to the p-wave potential scattering from Pb^{206} and by the cross sections of the less abundant isotopes. The radio-lead samples were thin since they were used as the compensators for the natural lead; therefore the statistical error in the cross section is large. For this reason, as well as the very close level spacing, no detailed analysis was attempted on the radio-lead.

According to shell theory, the level density increases rapidly with increasing excitation energy. The wide level spacing observed in the compound nucleus Pb^{209} is consistent with its low binding energy (3.87 Mev) as compared to the higher values found for other lead isotopes (6.73 Mev for Pb^{207} and 7.38 Mev for Pb^{208}) and most other heavy nuclei. This low bind-

ing energy is to be expected on the basis of the idea of the existence of closed shells in nuclei.[29] (Pb^{208} is doubly "magic" in that 82 protons and 126 neutrons form closed shells.) The narrow level spacing in the compound nucleus Pb^{207} is observed from the radio-lead cross section shown in Figure 12.

Figure 12

CROSS SECTION CURVE FOR RADIO-LEAD

RADIO LEAD

206 - 88 %
207 - 9 %
208 - 3 %

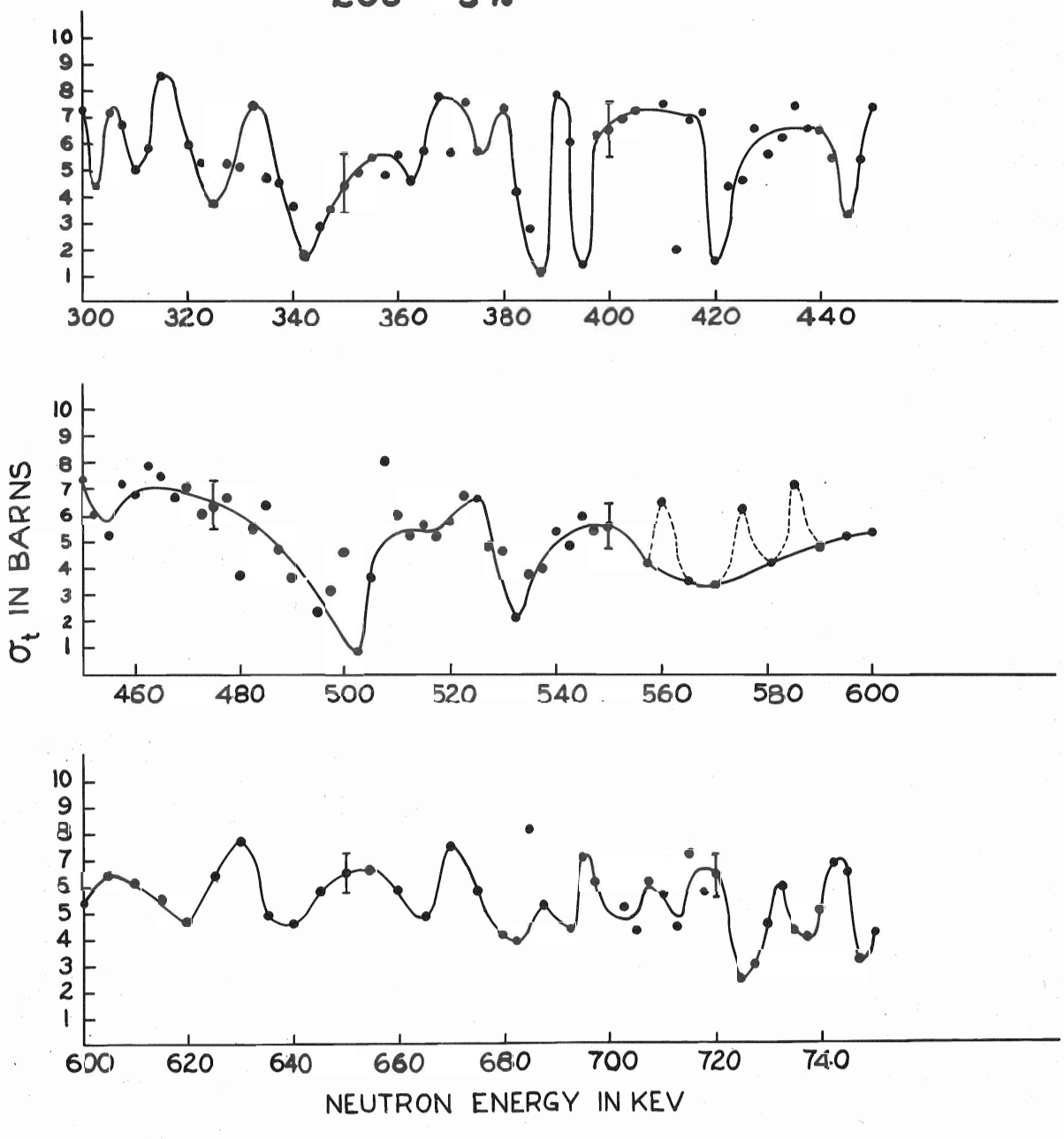

BIBLIOGRAPHY

BIBLIOGRAPHY

(1) Blatt, J. M., and V. F. Weisskopf, Theoretical Nuclear Physics, (John Wiley and Sons, New York, 1952).

(2) Cranberg, L., R.K. Beauchamp, and J. S. Levin, New System for Measurement of Fast Neutron Total Cross Sections, Los Alamos Scientific Laboratory.

(3) Hibdon, Carl T., Phys. Rev. 108, 414 (1957).

(4) Batchelor, R. B., Proc. Phys. Soc. (London) A68, 452 (1955).

(5) Bevington, P. R., G. E. Mitchell, W. W. Rolland, R. M. Wilenzick, and H. W. Lewis, (unpublished).

(6) Batchelor, R. B., and G. C. M. Morrison, Proc. Phys. Soc. (London) A68, 1081 (1955).

(7) Barschall, H. H., C. K. Bockelman, R. E. Peterson, and R. K. Adair, Phys. Rev. 76, 1146 (1949).

(8) Peterson, R. E., R. K. Adair, and H. H. Barschall, Phys. Rev. 79, 935 (1950).

(9) Breit, G., and E. Wigner, Phys. Rev. 49, 519 (1936).

(10) Bethe, H., and G. Placzek, Phys. Rev. 51, 450 (1937).

(11) Feshbach, H., D. Peaslee, and V. F. Weisskopf, Phys. Rev. 71, 145 (1947).

(12) Final Report of the Fast Neutron Data Project, 1951, Atomic Energy Commission, Report NYO-636.

(13) Feshbach, H., C. E. Porter, and V. F. Weisskopf, Phys. Rev. 96, 448 (1954).

(14) Adair, R. K., Rev. Modern Phys. 22, 249 (1950).

(15) Wigner, E. P., Am. J. Phys. 17, 99 (1949).

(16) Hughes, D. J., Neutron Cross Sections, (Pergamon Press, New York, 1957).

(17) Warren, R. E., J. L. Powell, and R. G. Herb, Rev. Sci. Ins. 18, 559 (1947).

(18) Parks, P. B., H. W. Newson, and R. M. Williamson, Bull. Amer. Phys. Soc. 3, 164 (1958).
Also Rev. Sci. Ins. (to be published).

(19) Weber, W., C. W. Johnstone, and L. Cranberg, Rev. Sci. Ins. 27 166 (1956).

(20) Hansen, A. O., and J. L. McKibben, Phys. Rev. 72, 673 (1947).

(21) Taschek, R. F., and A. Hemmindinger, Phys. Rev. 74, 373 (1948).

(22) Herb, R. G., S. C. Snowden, and O. Sala, Phys. Rev. 75 246 (1949).

(23) Ajzenberg, F., and T. Lauritsen, Rev. Modern Phys. 27, 77 (1955).

(24) Seidl, F. G. P., D. J. Hughes, H. Palevsky, J. S. Levin, W. Y. Kato, and N. G. Sjostrand, Phys. Rev. 95, 476 (1954).

(25) Seth, K. K., Phys. Rev. Letters (to be published).

(26) Seth, K. K., and H. W. Newson (to be published).

(27) Evans, R. D., The Atomic Nucleus, (McGraw-Hill, New York, 1955).

(28) Seth, K. K., oral communication.

(29) Mayer, M. G., and J. H. D. Jenson, Elementary Theory of Nuclear Shell Structure, (John Wiley and Sons, Inc., New York) 1955.